Geochemical Perspectives Letters

© 2026 The Authors
Published by the European Association of Geochemistry

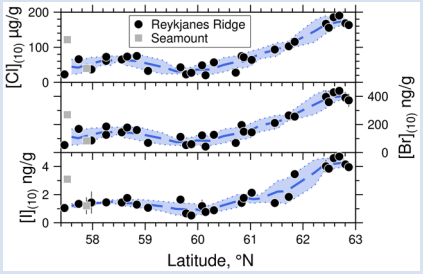
Halogens track mantle enrichment along the Reykjanes Ridge towards Iceland

E.C. Waters[1,2], R. Burgess[1], L. Ruzié-Hamilton[1], O. Shorttle[3,4], S.A. Halldórsson[5], M.E. Hartley[1*]

OPEN ACCESS

https://doi.org/10.7185/geochemlet.2640

Abstract



Halogens enter the mantle by subduction of altered oceanic crust, and return to the exosphere through magmatic degassing. Submarine basaltic glasses from the Reykjanes Ridge sample a 700 km transect towards the Iceland plume, capturing a transition from depleted towards strongly plume-influenced mantle. Chlorine, Br and I concentrations increase sharply as the mantle becomes more enriched, matching the behaviour of lithophile trace elements and radiogenic isotopes. Halogen enrichment does not correlate with $^{3}He/^{4}He$, suggesting that the halogen budget of Reykjanes Ridge magmas approaching Iceland is controlled by an enriched upper mantle component, not by the high-$^{3}He/^{4}He$ plume source. This enriched mantle likely contains 33–61 µg/g Cl, 77–149 ng/g Br and 0.8–1.6 ng/g I, with most of this halogen inventory derived from recycled oceanic crust.

Received 8 May 2026 | Accepted 21 September 2026 | Published 4 November 2026

Introduction

The flux of volatile elements into the mantle *via* subduction has created significant geochemical heterogeneity in the deep Earth over geological time (*e.g.*, Bekaert *et al.*, 2024). The fluid-mobile and highly incompatible halogens (Cl, Br, I) are significantly enriched in seawater, sediments, altered oceanic crust and serpentinised lithosphere compared to depleted upper mantle (Barnes *et al.*, 2018). Although halogens from subducting slabs are lost to the mantle wedge and arc magmatism, primarily *via* slab dehydration, exhumed high-pressure antigorite serpentinites can retain significant halogen concentrations (John *et al.*, 2011). The stability of antigorite to depths of 150–200 km (Ulmer and Trommsdorff, 1995) suggests that slab residues have capacity to return a significant flux of halogens to the deep mantle (Barnes *et al.*, 2018), making halogens potentially powerful tracers of recycled subducted lithologies.

Diverse halogen enrichments and $\delta^{37}Cl$ values have been observed among plume settings (*e.g.*, John *et al.*, 2010; Kendrick *et al.*, 2015; Halldórsson *et al.*, 2016a), implying variability in the efficiency of the solid Earth halogen cycle in space and/or time. The Iceland mantle plume, as the largest modern expression of a deep mantle upwelling (Hoggard *et al.*, 2016) and known to return recycled material to the surface (Shorttle and Maclennan, 2011), provides an excellent opportunity to evaluate the solid Earth halogen cycle.

We report halogen (Cl, Br, I) compositions in 29 basalt glasses dredged from the Reykjanes Ridge between 57.4° N and 63° N during the RSS Charles Darwin cruise CD80 (Murton *et al.*, 2002) (Fig. S-1). The Reykjanes Ridge lies in a region of the North Atlantic with positive residual depth and V-shaped ridges manifest, preserving an indirect record of thermal pulsing of the Iceland plume over time (Parnell-Turner *et al.*, 2017). It samples along-ridge mantle heterogeneity associated with the Iceland plume, as well as local heterogeneity in adjacent seamounts. Lithophile trace element and isotopic signatures (*e.g.*, Murton *et al.*, 2002) indicate the progressive melting out of enriched domains as the mantle flows radially outwards from the Iceland plume and through the melting region of the Reykjanes Ridge (Shorttle *et al.*, 2010), until by 61° N the fingerprint of trace element and isotopic enrichment is gone. A broad peak in $^{3}He/^{4}He$ (16.0 R/R_A) at 59–62° N coincides with the first V-shaped ridge, while elevated $^{3}He/^{4}He$ above 11 R/R_A persists as far south as 57° N (Hilton *et al.*, 2000). To a first order, these observations suggest a heterogeneous plume in which lithophile element and helium isotopic signatures are carried by different mantle components, with the high-$^{3}He/^{4}He$ component becoming visible once the enriched component(s) is exhausted and/or at very high temperatures of melting (*e.g.*, Rasmussen *et al.*, 2020). Icelandic basalts are overall geochemically depleted and exhibit neither extreme EM nor HIMU compositions (*e.g.*, Harðardóttir *et al.*, 2022); however, their trace element and isotopic heterogeneity requires at least two depleted and three

1. Deparment of Earth and Environmental Sciences, University of Manchester, Oxford Road, Manchester, M13 9PL, UK
2. School of Geographical and Earth Sciences, University of Glasgow, Lilybank Gardens, Glasgow, G12 8RZ, UK
3. Department of Earth Sciences, University of Cambridge, Downing Street, Cambridge, CB2 3EQ, UK
4. Institute of Astronomy, University of Cambridge, Madingley Rise, Cambridge, CB3 0HA, UK
5. Nordic Volcanological Center, Institute of Earth Sciences, University of Iceland, 102 Reykjavík, Iceland
* Corresponding author (email: margaret.hartley@manchester.ac.uk)

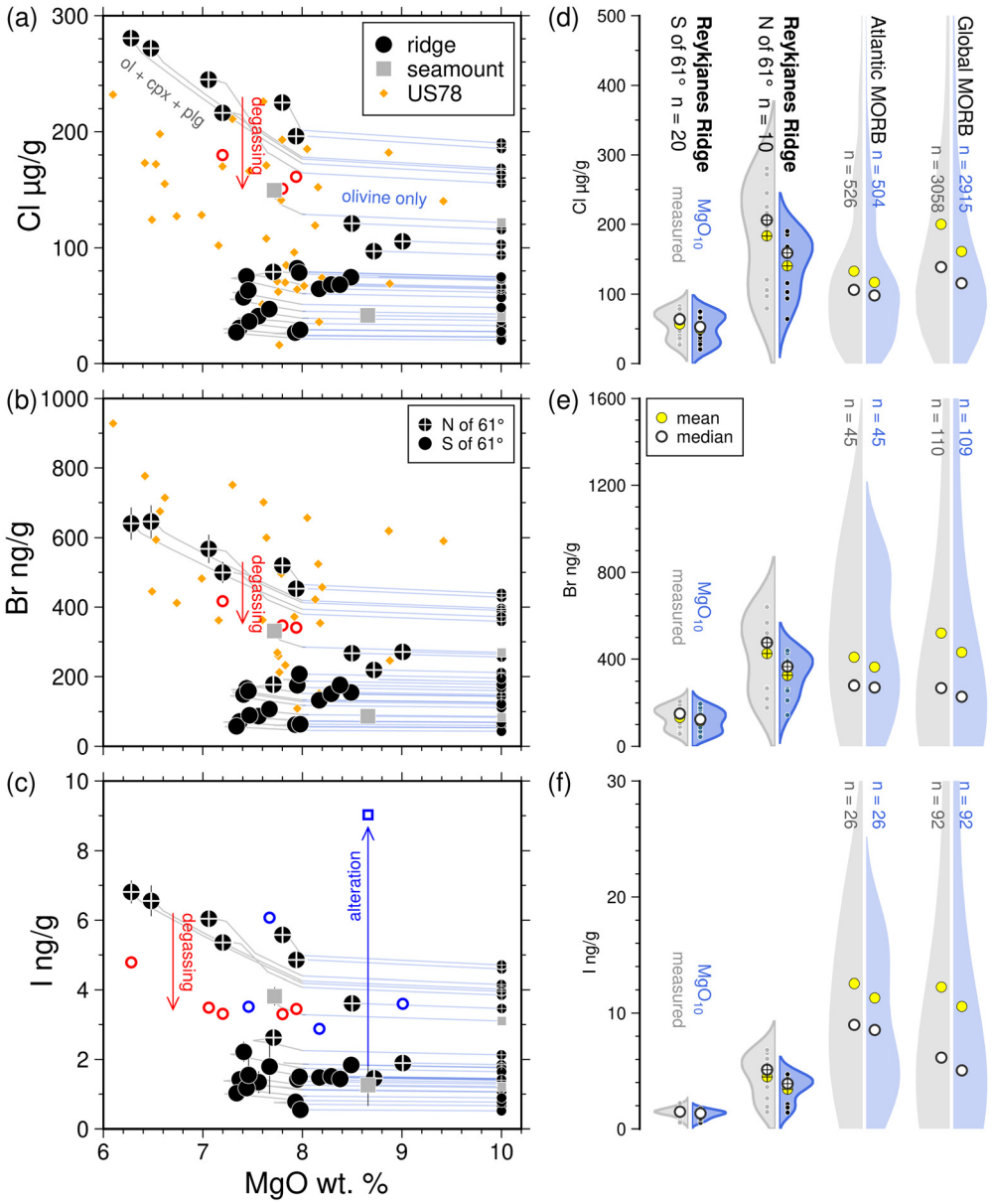


Figure 1 **(a–c)** Halogen contents in Reykjanes Ridge glasses from 57.4–63° N *vs.* MgO, with reverse fractional crystallisation paths to 10 wt. % MgO. Crossed symbols indicate samples from the northern Reykjanes Ridge ≥61° N. Open symbols show glass compositions without correction for degassing (red) or alteration (blue). Orange diamonds are Reykjanes Ridge whole rocks from 57.7–63.8° N (US78; Unni and Schilling, 1978). **(d–f)** Kernel density distributions of glass compositions as measured (left, grey; note change of *y* axis scale), and after correction to 10 wt. % MgO (right, blue). Southern (<61° N) and northern segments of the Reykjanes Ridge are compared with Atlantic and global MORB (data compiled from PetDB, www.earthchem.org/petdb).

enriched local mantle endmembers with weak but variable EM1- or HIMU-like affinities (*e.g.*, Peate *et al.*, 2010). We aim to constrain the relative contributions of enriched, depleted and high-$^{3}He/^{4}He$ mantle endmembers to the halogen budget of Reykjanes Ridge magmas.

Halogen Abundances in Reykjanes Ridge Glasses

We measured Cl, Br, I and K in fresh glass chips by neutron irradiation noble gas mass spectrometry (Ruzié-Hamilton *et al.*, 2016). Analytical and data reduction procedures, and complete datasets, are provided as Supplementary Information. Typical 1σ uncertainties are ±1–3 µg/g for Cl, ±5–40 ng/g for Br, ±0.05–0.30 ng/g for I, and ±1–10 µg/g for K. From a mantle geochemical perspective, it is important to ascertain whether halogen contents were modified by magma degassing or assimilation of seawater or brines. We corrected five samples for degassing and five for alteration. Following corrections, pristine Reykjanes Ridge glasses contain 26–281 µg/g Cl, 57–646 ng/g Br, 0.5–9.0 ng/g I, and 270–1580 µg/g K. Negative correlations between MgO and halogens in glasses from the northern Reykjanes Ridge ≥61° N (Fig. 1a–c) are well explained as incompatible element enrichment by exclusion during fractional crystallisation, arguing strongly against an assimilation origin for the elemental halogen variability in these samples.

To explore mantle-derived variability in primary melt halogen contents we correct all Reykjanes Ridge glasses to 10 wt. % MgO. This yields primary melt halogen abundances of 20–190 µg/g Cl, 43–440 ng/g Br and 0.5–4.7 ng/g I (Fig. 1).

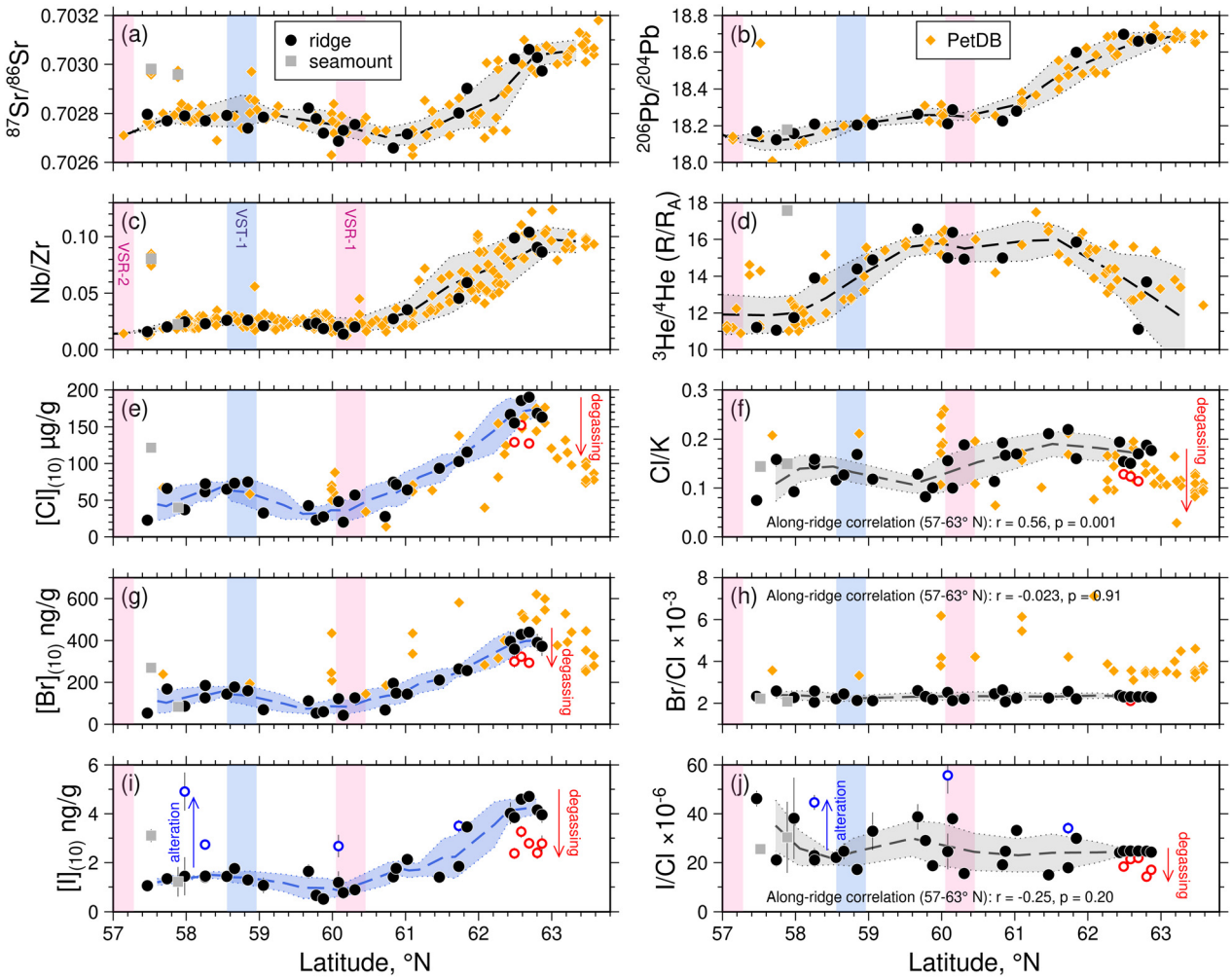


Figure 2 Along-ridge compositional variation in Reykjanes Ridge glasses. **(a)** $^{87}Sr/^{86}Sr$, **(b)** $^{206}Pb/^{204}Pb$, **(c)** Nb/Zr, **(d)** $^{3}He/^{4}He$ (R/R_A notation), **(e, g, h)** halogen concentrations after fractionation correction to 10 wt. % MgO (halogen contents without fractionation correction are shown in Fig. S-7), and **(f)** Cl/K, **(h)** Br/Cl, **(j)** I/Cl ratios (no fractionation correction). Vertical bands: V-shaped ridges (VSR, pink) and troughs (VST, blue). Open red and blue symbols as for Figure 1. Dashed lines and shaded areas show the along-ridge running average and 1σ standard deviation, calculated using a boxcar filter with bandwidth 2° latitude. Reykjanes Ridge glass and whole-rock compositions (orange diamonds) are compiled from PetDB; Br and Cl (Unni and Schilling, 1978) are not corrected for the effects of degassing or alteration.

Samples from <61° N have lower mean and median halogen contents than Atlantic and global MORB (Fig. 1d–f). All Reykjanes Ridge basalts have lower I contents than Atlantic or global MORB, although the broad MORB composition distributions extending to 30 ng/g I (Fig. 1f) likely include samples affected by alteration.

Along-Ridge Variations in Halogen Geochemistry

Fractionation-corrected Cl, Br and I contents show significant along-ridge enrichments north of 61° N (Figs. 2e,g,i, S-7), and correlate positively with radiogenic isotopic signatures (Figs. 2a,b, S-8); incompatible trace element abundances; and ratios of similarly incompatible trace elements such as Nb/Zr (Figs. 2c; S-8). South of 61° N, halogens and Cl/K co-vary with Sr isotopes and Nb/Zr in a broad swell centred around 58.7° N (Fig. 2). This region includes two enriched seamounts, one of which has high halogen abundances (Fig. 2).

South of 61° N, the mean Cl/K = 0.13 ± 0.04 and mean Br/K = (0.31 ± 0.09) × 10^{-3} are higher than reported for global MORB (Kendrick, 2024) but overlap within 1σ; the mean I/K = (3.4 ± 0.7) × 10^{-6} lies towards the lower end of the global MORB range. Halogen/K ratios show statistically significant along-ridge increases between 57.4° N and 63° N (*e.g.*, Cl/K rises from ~0.1 to ~0.19; Fig. 2f), but halogen/halogen ratios remain constant (Fig. 2h,j). The near doubling of halogen abundances with respect to K cannot be explained by simple fractionation control. These along-ridge geochemical associations indicate that the high halogen budgets of basalts from ≥61° N are strongly controlled by the influence of an enriched upper mantle component that is inherently halogen-rich compared to local depleted mantle.

Reykjanes Ridge Halogen Ratios are Mantle-Like

Potassium, Cl, Br and I have similar partition coefficients during mantle melting (Kendrick *et al.*, 2012); thus, melt halogen/K and halogen/halogen ratios should reflect their mantle source. Reykjanes Ridge glasses show mantle-like Br/Cl and H_2O/Cl, and their I/Cl and K/Cl overlap global MORB and the lower bounds of mantle ranges (Fig. 3).

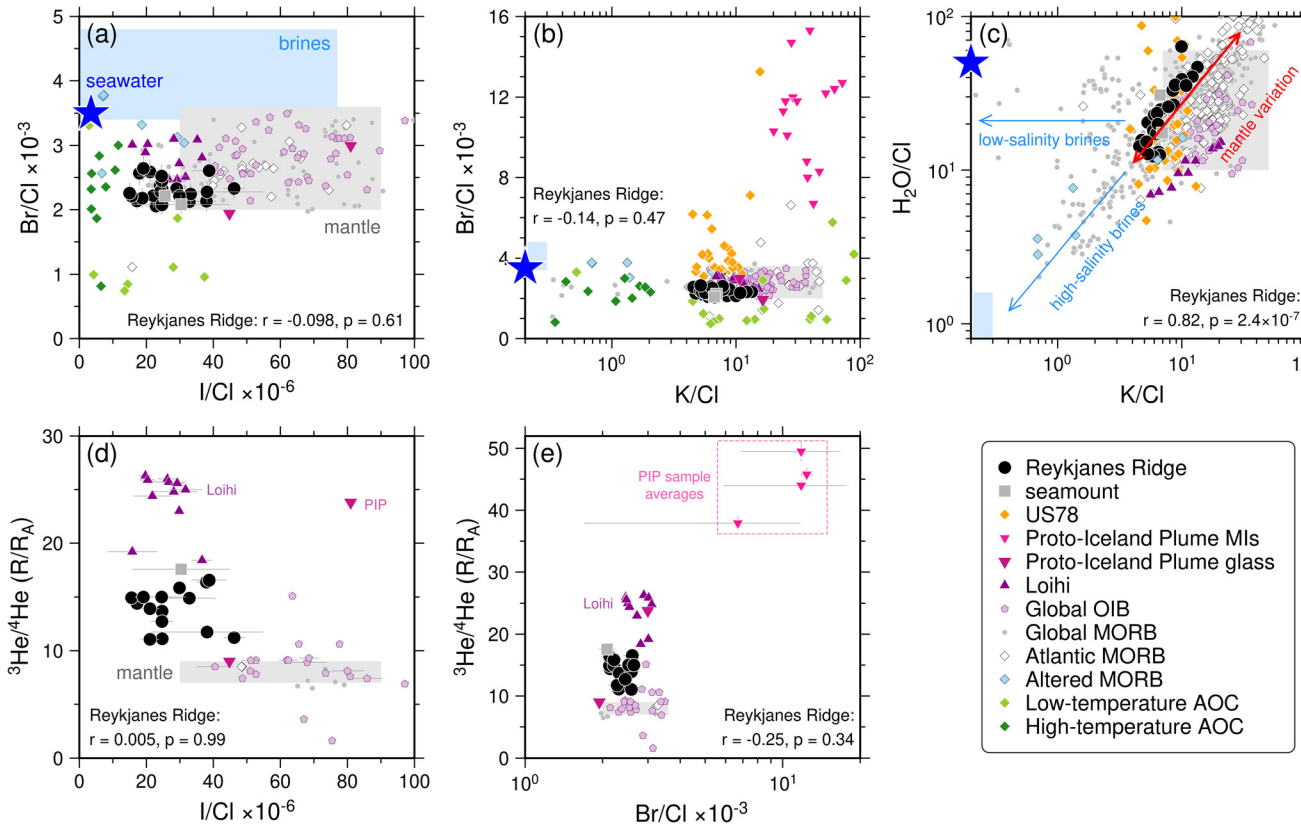


Figure 3 Compositions of Reykjanes Ridge glasses (this study) and whole rocks (US78; Unni and Schilling, 1978) compared with proto-Iceland plume melt inclusions (MI; Tomlinson *et al.*, 2025), glasses from Lō'ihi (Kendrick *et al.*, 2025), global MORB and OIB, and altered oceanic crust (AOC). Data sources listed in Table S-2.

High Cl/K in Reykjanes Ridge glasses has previously been interpreted as indicating seawater-derived Cl enrichment *via* assimilation of hydrothermally altered material (Michael and Cornell, 1998). High-temperature alteration of basalt and dolerite in the upper oceanic crust may lead to K and I leaching coupled with crystallisation of Cl-rich amphiboles, producing high bulk Cl/K and low I/Cl compared to fresh MORB (Chavrit *et al.*, 2016). However, Reykjanes Ridge Br/Cl, I/Cl and K/Cl are not correlated, and are not similar to altered oceanic crust (Fig. 3). Likewise, systematic covariation of halogens, Sr and Pb isotopes, and Nb/Zr (Fig. 2) indicates no role for progressive seawater assimilation with proximity to Iceland. We therefore interpret our Reykjanes Ridge halogen/halogen and halogen/K ratios as primary and mantle-derived. The high Cl/K suggests that the enriched upper mantle component sampled by the northern Reykjanes Ridge tends toward weak HIMU affinity (*e.g.*, Kendrick, 2024 and references therein).

Helium isotopes are decoupled from trace elements and halogen enrichments (Fig. 2) and show no relationship with halogen/halogen or halogen/K ratios (Figs. 3d,e, S-8 and S-9). Helium concentrations decrease due to pre-eruptive magmatic degassing as eruption depth shallows from ~2 km at 57.4° N to ~300 m at 63° N (Hilton *et al.*, 2000), but degassing is not expected to fractionate $^{3}He/^{4}He$. Lower $^{3}He/^{4}He$ in the northern ridge segment ≥61° N can be attributed to the addition of radiogenic crustal helium to already-degassed magmas (Hilton *et al.*, 2000), obscuring mantle-derived $^{3}He/^{4}He$ signatures. However, the absence of correlation between halogen abundances and $^{3}He/^{4}He$ persists even if samples from ≥61° N are excluded (Fig. S-8). Olivine-hosted melt inclusions in high-$^{3}He/^{4}He$ proto-Iceland plume (PIP) basalts from Baffin Island and West Greenland exhibit high Br/Cl (Tomlinson *et al.*, 2025), but this signature is absent from the moderate-$^{3}He/^{4}He$ Reykjanes Ridge glasses (Figs. 3e, S-8). Reykjanes Ridge glasses have low I/Cl similar to glasses from Lō'ihi (Kendrick *et al.*, 2025), but are unlike high-$^{3}He/^{4}He$ PIP glass which has high I/Cl (Fig. 3d). Taken together, these observations suggest that Iceland's high-$^{3}He/^{4}He$ mantle contributes minimally to the halogen budget of Reykjanes Ridge magmas, and consequently that low I/Cl is intrinsic to the Reykjanes Ridge mantle rather than associated with the high-$^{3}He/^{4}He$ component.

Halogen Abundances of Enriched and Depleted Primary Melts along the Reykjanes Ridge

Our data suggest that the halogen contents of Reykjanes Ridge basalts are relatively insensitive to the complex multi-component heterogeneity of the Iceland plume and can, to a first order, be modelled as binary mixtures of depleted and enriched endmember melts. This affords an opportunity to calculate a predicted halogen budget for Iceland's most enriched basalts. To do this, we take the average composition of Reykjanes Ridge basalts south of 61° N as the depleted melt endmember, and for the enriched endmember we select the onland Stapafell subglacial formation (Fig. S-1) because it continues the towards-Iceland geochemical enrichment trends set by the Reykjanes Ridge (Novella *et al.*, 2020). Stapafell basalts (8.3 wt. % MgO) represent some of the most enriched compositions in Iceland's neovolcanic rift zones: they have $^{3}He/^{4}He \approx 14\ R/R_A$ (Halldórsson *et al.*, 2016b) and high incompatible element contents, low $^{143}Nd/^{144}Nd \approx 0.5013$ and high $^{206}Pb/^{204}Pb \approx 18.9$

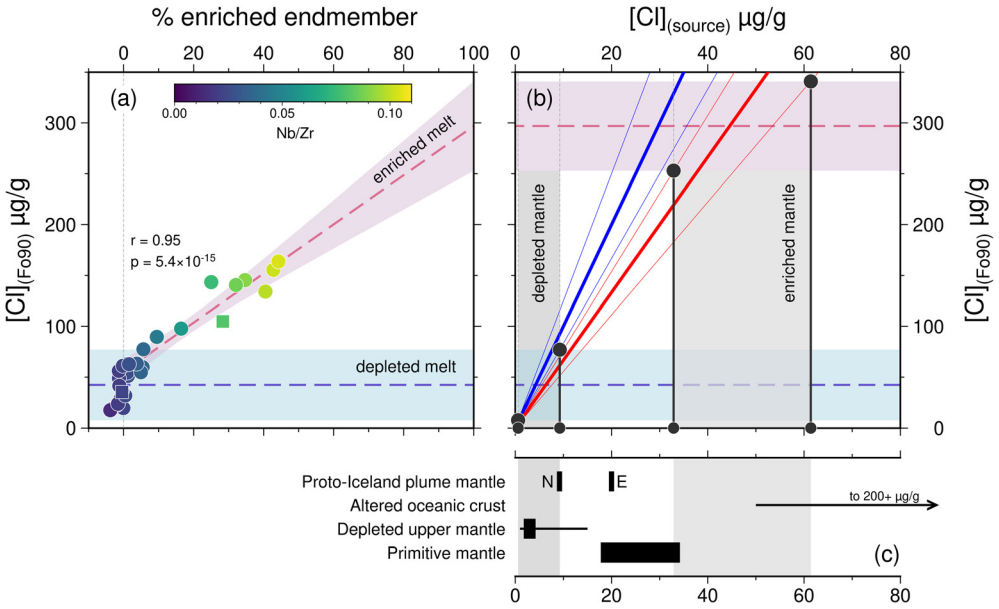


Figure 4 **(a)** The proportion of enriched melt contributing to Reykjanes Ridge basalts is regressed against the fractionation-corrected $[Cl]_{(Fo90)}$. Shaded area shows 95 % confidence interval on the best-fit regression. Right-most edge of the plot indicates the expected Cl content of enriched Icelandic basalts as represented by Stapafell. **(b)** An aggregate fractional melting model is used to link depleted and enriched primary melt compositions with plausible mantle source compositions, $[Cl]_{(source)}$. Blue lines show aggregate melt compositions for spinel lherzolite, calculated for melt fractions $0.08 < F < 0.12$ with $D_{Cl}^{bulk} = 0.0015$. Red lines show aggregate melt compositions for an enriched pyroxenite ($0.13 < F < 0.18$; $D_{Cl}^{bulk} = 0.0197$). Vertical grey bars mark viable mantle source compositions that, for the stated assumptions regarding F and D_{Cl}^{bulk}, could produce the depleted and enriched primary melt compositions. **(c)** Viable mantle source Cl contents are compared with published mantle compositions and altered oceanic crust. Data sources listed in Table S-7. Equivalent figures for Br and I are provided as Supplementary Information.

(Peate *et al.*, 2009) that could be interpreted as consistent with either very weak EM1 or HIMU affinity.

We use the incompatible trace element ratio Nb/Zr as a proxy for enrichment (Shorttle and Maclennan, 2011). Reykjanes Ridge basalts south of 61° N have mean Nb/Zr = 0.02 (Murton *et al.*, 2002); Stapafell basalts have Nb/Zr = 0.159 (Peate *et al.*, 2009). We use mass balance to constrain the mass fraction of enriched melt that must be added to ambient Reykjanes Ridge depleted melt to produce the observed Nb/Zr for each Reykjanes Ridge sample. Calculated contributions from the enriched endmember are then plotted against sample halogen contents that are fractionation-corrected to be in equilibrium with Fo_{90} mantle olivine (Fig. 4a), and best-fit regression is used to constrain the halogen content of the enriched primary melt. Depleted Reykjanes Ridge primary melts are constrained by our samples to contain 7.5–75 µg/g Cl (Fig. 4a), 55–140 ng/g Br and 0.75–1.35 ng/g I. Enriched Stapafell-like primary melts are projected to contain 215–340 µg/g Cl (Fig. 4a), 590–830 ng/g Br and 6.5–9.1 ng/g I.

Halogen Abundances of Enriched and Depleted Mantle Sources Supplying the Reykjanes Ridge

We next project the depleted and enriched primary melt compositions into plausible estimates of the halogen contents of their respective mantle sources. We constructed an aggregate fractional melting model to constrain the mantle lithology, composition and melting degree that best reproduce the trace element systematics of Reykjanes Ridge and Stapafell basalts (Supplementary Information). Halogens are incorporated into the melting model by calculating suitable partition coefficients based on mineral-melt partitioning experiments (Joachim *et al.*, 2015), and assuming that $D_{Cl}^{bulk} = D_{Br}^{bulk} = D_{I}^{bulk}$.

Trace element systematics of Reykjanes Ridge basalts south of 61° N are reproduced by 8–13 % melting of depleted spinel peridotite (Fig. S-10), consistent with previous estimates (Murton *et al.*, 2002). Taking this mantle lithology and range of melting degrees, and using our estimated halogen contents for depleted primary melts along the Reykjanes Ridge as input liquid compositions, we calculate that the depleted mantle sourcing these melts contains 1–10 µg/g Cl (Fig. 4b), 4–17 ng/g Br and 0.06–0.16 ng/g I; all are within published estimates for the upper mantle (Kendrick, 2024). Setting melting degree to $F = 0.1$ we obtain preferred $Br/Cl = 2.3 \times 10^{-3}$ and $I/Cl = 25 \times 10^{-6}$ (Table S-6).

Trace element systematics of enriched Stapafell-like magmas are best reproduced by a more complex melting model in which instantaneous melts from a Reykjanes Ridge-like depleted mantle mix with melts of a more enriched upper mantle component (Novella *et al.*, 2020) – a scenario similar to that proposed for the 2021 Fagradalsfjall eruption (Marshall *et al.*, 2024). To bracket plausible halogen contents for the enriched mantle, we require reasonable assumptions regarding its lithology, composition and melting degree. To calculate lower-bound halogen abundances we consider 13 % melting of primitive spinel pyroxenite, and for the upper bound we consider 18 % melting of primitive garnet pyroxenite. These lithologies and melting degrees closely match those chosen by Shorttle *et al.* (2015) as reasonable estimates given the requirement for melting model results to match along-ridge crustal thickness variations. Using these assumptions, we calculate that the enriched Icelandic mantle component, as represented by Stapafell, could contain 33–61 µg/g Cl (Fig. 4b), 77–149 ng/g Br and 0.8–1.6 ng/g I (Table S-6). These Cl and Br contents overlap upper estimates for primitive mantle

and lowermost estimates for altered oceanic crust (Figs. 4c, S-11c); the I content is lower than primitive mantle (7 ± 4 ng/g; Kendrick, 2024). Setting melting degree to $F = 0.15$ we obtain preferred Br/Cl = 2.4×10^{-3} and I/Cl = 26×10^{-6}, indistinguishable from depleted Reykjanes Ridge mantle. While our calculations cannot uniquely constrain the halogen budget of the enriched Icelandic mantle component, they illustrate the key parameters that must be considered in order to arrive at plausible estimates.

Despite the limitations of our modelling approach, our results strongly indicate that the enriched Icelandic mantle component is halogen-rich compared to depleted Reykjanes Ridge mantle. This enriched component is well matched by a refertilised pyroxenite containing up to 50 % recycled subducted oceanic crust, *i.e.* the KG1 lithology (Shorttle and Maclennan, 2011). Thus, we propose that the high halogen inventory of enriched Icelandic melts can be attributed to recycled oceanic crust in the mantle source. This recycled component is constrained to be as young as Phanerozoic in age (Halldórsson *et al.*, 2016b, and references therein). Strong positive correlations between halogens, radiogenic isotopes and the proportion of enriched melt (Figs. 3, S-8) reveal that high halogen abundances are characteristic fingerprints of recycled oceanic crust. In contrast, enriched Icelandic and depleted Reykjanes Ridge mantle have near-identical Br/Cl and I/Cl, despite their differing halogen contents. This is consistent with halogens being minimally fractionated from one another during subduction processing and/or in the upper mantle during mixing and dilution of subducted materials with halogen-poor depleted peridotite over geological time (*e.g.*, Kendrick, 2024). Our preferred I/Cl lies slightly below mantle estimates, suggesting that at least some global-scale heterogeneity of halogen ratios is retained in the upper mantle and recovered at the surface in erupted basalt compositions.

Conclusions and Implications

We have constrained the halogen budget of an enriched upper mantle component that contributes significantly to trace element, radiogenic isotope and halogen enrichment in Reykjanes Ridge basalts approaching Iceland. The halogen signature of Iceland's high-^{3}He/^{4}He plume source is not resolved in our data, suggesting that Iceland's high-^{3}He/^{4}He mantle may be halogen-poor, similar to the Cl- and strongly I-depleted Lō'ihi source (Kendrick *et al.*, 2025), and that low I/Cl is intrinsic to local Reykjanes Ridge mantle. The I/Cl signature of Iceland's high-^{3}He/^{4}He plume remains to be characterised, leaving open the possibility that halogen depletions and low I/Cl are characteristic of global high-^{3}He/^{4}He mantle sources.

Acknowledgements

The authors thank Mark Kendrick, Emma Tomlinson, an anonymous reviewer, and handling editor Ambre Luguet, for their thoughtful reviews. This work was funded by NERC grant NE/P002331/1 and a NERC studentship to ECW through the Manchester-Liverpool Doctoral Training Partnership NE/L002469/1. We acknowledge support from NERC grants NE/T012455/1 (OS), NE/V011383/1 (OS), NE/V010905/1 (MEH), and NE/X01642/1 (MEH, RB). We thank Lydia Fawcett for assistance with sample irradiation and NI-NGMS analyses. We acknowledge the National Oceanographic Centre, the PETROS project, and Bramley Murton for access to the Reykjanes Ridge samples.

Editor: Ambre Luguet

Additional Information

Supplementary Information accompanies this letter at https://www.geochemicalperspectivesletters.org/article2640.

© 2026 The Authors. This work is distributed under the Creative Commons Attribution 4.0 License, which permits unrestricted use, distribution, and reproduction in any medium, provided the original author and source are credited. Additional information is available at http://www.geochemicalperspectivesletters.org/copyright-and-permissions.

Cite this letter as: Waters, E.C., Burgess, R., Ruzié-Hamilton, L., Shorttle, O., Halldórsson, S.A., Hartley, M.E. (2026) Halogens track mantle enrichment along the Reykjanes Ridge towards Iceland. *Geochem. Persp. Let.* 42, 39–45. https://doi.org/10.7185/geochemlet.2640

References

Barnes, J.D., Manning, C.E., Scambelluri, M., Selverstone, J. (2018) The Behavior of Halogens During Subduction-Zone Processes. In: Harlov, D.E., Aranovich, L. (Eds.) *The Role of Halogens in Terrestrial and Extraterrestrial Geochemical Processes: Surface, Crust and Mantle*. Springer Geochemistry, Cham, 545–590. https://doi.org/10.1007/978-3-319-61667-4_8

Bekaert, D.V., Barry, P.H., Curtice, J., Blusztajn, J., Hudak, M., *et al.* (2024) A carbon, nitrogen, and multi-isotope study of basalt glasses near 14°N on the Mid-Atlantic Ridge. Part B: Mantle source heterogeneities. *Geochimica et Cosmochimica Acta* 369, 179–195. https://doi.org/10.1016/j.gca.2023.12.017

Chavrit, D., Burgess, R., Sumino, H., Teagle, D.A.H., Droop, G., Shimizu, A., Ballentine, C.J. (2016) The contribution of hydrothermally altered ocean crust to the mantle halogen and noble gas cycles. *Geochimica et Cosmochimica Acta* 183, 106–124. https://doi.org/10.1016/j.gca.2016.03.014

Halldórsson, S.A., Barnes, J.D., Stefánsson, A., Hilton, D.R., Hauri, E.H., Marshall, E.W. (2016a) Subducted lithosphere controls halogen enrichments in the Iceland mantle plume source. *Geology* 44, 679–682. https://doi.org/10.1130/G37924.1

Halldórsson, S.A., Hilton, D.R., Barry, P.H., Füri, E., Grönvold, K. (2016b) Recycling of crustal material by the Iceland mantle plume: New evidence from nitrogen elemental and isotope systematics of subglacial basalts. *Geochimica et Cosmochimica Acta* 176, 206–226. https://doi.org/10.1016/j.gca.2015.12.021

Harðardóttir, S., Matthews, S., Halldórsson, S.A., Jackson, M.G. (2022) Spatial distribution and geochemical characterization of Icelandic mantle endmembers: Implications for plume geometry and melting processes. *Chemical Geology* 604, 120930. https://doi.org/10.1016/j.chemgeo.2022.120930

Hilton, D.R., Thirlwall, M.F., Taylor, R.N., Murton, B.J., Nichols, A. (2000) Controls on magmatic degassing along the Reykjanes Ridge with implications for the helium paradox. *Earth and Planetary Science Letters* 183, 43–50. https://doi.org/10.1016/S0012-821X(00)00253-3

Hoggard, M.J., White, N., Al-Attar, D. (2016) Global dynamic topography observations reveal limited influence of large-scale mantle flow. *Nature Geoscience* 9, 456–463. https://doi.org/10.1038/ngeo2709

Joachim, B., Pawley, A., Lyon, I.C., Marquardt (neé Hartmann), K., Henkel, T., Clay, P.L., Ruzié, L., Burgess, R., Ballentine, C.J. (2015) Experimental partitioning of F and Cl between olivine, orthopyroxene and silicate melt at Earth's mantle conditions. *Chemical Geology* 416, 65–78. https://doi.org/10.1016/j.chemgeo.2015.08.012

John, T., Layne, G.D., Haase, K.M., Barnes, J.D. (2010) Chlorine isotope evidence for crustal recycling into the Earth's mantle. *Earth and Planetary Science Letters* 298, 175–182. https://doi.org/10.1016/j.epsl.2010.07.039

John, T., Scambelluri, M., Frische, M., Barnes, J.D., Bach, W. (2011) Dehydration of subducting serpentinite: Implications for halogen mobility in subduction zones and the deep halogen cycle. *Earth and Planetary Science Letters* 308, 65–76. https://doi.org/10.1016/j.epsl.2011.05.038

Kendrick, M.A. (2024) Halogen Cycling in the Solid Earth. *Annual Review of Earth and Planetary Sciences* 52, 195–220. https://doi.org/10.1146/annurev-earth-031621-111700

Kendrick, M.A., Kamenetsky, V.S., Phillips, D., Honda, M. (2012) Halogen systematics (Cl, Br, I) in Mid-Ocean Ridge Basalts: A Macquarie Island case study.

Geochimica et Cosmochimica Acta 81, 82–93. https://doi.org/10.1016/j.gca.2011.12.004

Kendrick, M.A., Jackson, M.G., Hauri, E.H., Phillips, D. (2015) The halogen (F, Cl, Br, I) and H_2O systematics of Samoan lavas: Assimilated-seawater, EM2 and high-$^3He/^4He$ components. *Earth and Planetary Science Letters* 410, 197–209. https://doi.org/10.1016/j.epsl.2014.11.026

Kendrick, M.A., Nebel, O., Hanyu, T., Maunder, B.L., Maas, R. (2025) Earth's early differentiation recorded by halogen abundance ratios in Hawaiian lavas. *Geochimica et Cosmochimica Acta* 393, 196–207. https://doi.org/10.1016/j.gca.2025.01.019

Marshall, E.W., Caracciolo, A., Bali, E., Halldórsson, S.A., Matthews, S., *et al.* (2024) The Petrology and Geochemistry of the 2021 Fagradalsfjall Eruption, Iceland: An Eruption Sourced From Multiple, Compositionally Diverse, Near-Moho Sills. *AGU Advances* 5, e2024AV001310. https://doi.org/10.1029/2024AV001310

Michael, P.J., Cornell, W.C. (1998) Influence of spreading rate and magma supply on crystallization and assimilation beneath mid-ocean ridges: Evidence from chlorine and major element chemistry of mid-ocean ridge basalts. *Journal of Geophysical Research: Solid Earth* 103, 18325–18356. https://doi.org/10.1029/98JB00791

Murton, B.J., Taylor, R.N., Thirlwall, M.F. (2002) Plume–Ridge Interaction: a Geochemical Perspective from the Reykjanes Ridge. *Journal of Petrology* 43, 1987–2012. https://doi.org/10.1093/petrology/43.11.1987

Novella, D., Maclennan, J., Shorttle, O., Prytulak, J., Murton, B.J. (2020) A multi-proxy investigation of mantle oxygen fugacity along the Reykjanes Ridge. *Earth and Planetary Science Letters* 531, 115973. https://doi.org/10.1016/j.epsl.2019.115973

Parnell-Turner, R., White, N., Henstock, T.J., Jones, S.M., Maclennan, J., Murton, B.J. (2017) Causes and Consequences of Diachronous V-Shaped Ridges in the North Atlantic Ocean. *Journal of Geophysical Research: Solid Earth* 122, 8675–8708. https://doi.org/10.1002/2017JB014225

Peate, D.W., Baker, J.A., Jakobsson, S.P., Waight, T.E., Kent, A.J.R., Grassineau, N.V., Skovgaard, A.C. (2009) Historic magmatism on the Reykjanes Peninsula, Iceland: a snap-shot of melt generation at a ridge segment. *Contributions to Mineralogy and Petrology* 157, 359–382. https://doi.org/10.1007/s00410-008-0339-4

Peate, D.W., Breddam, K., Baker, J.A., Kurz, M.D., Barker, A.K., Prestvik, T., Grassineau, N., Skovgaard, A.C. (2010) Compositional Characteristics and Spatial Distribution of Enriched Icelandic Mantle Components. *Journal of Petrology* 51, 1447–1475. https://doi.org/10.1093/petrology/egq025

Rasmussen, M.B., Halldórsson, S.A., Gibson, S.A., Guðfinnsson, G.H. (2020) Olivine chemistry reveals compositional source heterogeneities within a tilted mantle plume beneath Iceland. *Earth and Planetary Science Letters* 531, 116008. https://doi.org/10.1016/j.epsl.2019.116008

Ruzié-Hamilton, L., Clay, P.L., Burgess, R., Joachim, B., Ballentine, C.J., Turner, G. (2016) Determination of halogen abundances in terrestrial and extraterrestrial samples by the analysis of noble gases produced by neutron irradiation. *Chemical Geology* 437, 77–87. https://doi.org/10.1016/j.chemgeo.2016.05.003

Shorttle, O., Maclennan, J. (2011) Compositional trends of Icelandic basalts: Implications for short–length scale lithological heterogeneity in mantle plumes. *Geochemistry, Geophysics, Geosystems* 12, Q11008. https://doi.org/10.1029/2011GC003748

Shorttle, O., Maclennan, J., Jones, S.M. (2010) Control of the symmetry of plume-ridge interaction by spreading ridge geometry. *Geochemistry, Geophysics, Geosystems* 11, Q0AC05. https://doi.org/10.1029/2009GC002986

Shorttle, O., Moussallam, Y., Hartley, M.E., Maclennan, J., Edmonds, M., Murton, B.J. (2015) Fe-XANES analyses of Reykjanes Ridge basalts: Implications for oceanic crust's role in the solid Earth oxygen cycle. *Earth and Planetary Science Letters* 427, 272–285. https://doi.org/10.1016/j.epsl.2015.07.017

Tomlinson, E.L., Rose-Koga, E.F., Bouvier, A.-S., O'Farrell, D., Caulfield, J.T., Jackson, M.G., Moussallam, Y., Stuart, F.M., Villeneuve, J. (2025) Halogens in proto-Iceland plume basalts. *Geochemical Perspectives Letters* 37, 12–17. https://doi.org/10.7185/geochemlet.2539

Ulmer, P., Trommsdorff, V. (1995) Serpentine Stability to Mantle Depths and Subduction-Related Magmatism. *Science* 268, 858–861. https://doi.org/10.1126/science.268.5212.858

Unni, C.K., Schilling, J.-G. (1978) Cl and Br degassing by volcanism along the Reykjanes Ridge and Iceland. *Nature* 272, 19–23. https://doi.org/10.1038/272019a0

© 2026 The Authors

Halogens track mantle enrichment along the Reykjanes Ridge towards Iceland

E.C. Waters, R. Burgess, L. Ruzié-Hamilton, O. Shorttle, S.A. Halldórsson, M.E. Hartley

Supplementary Information

The Supplementary Information includes:

- 1. Sample Collection
- 2. Analytical Methods and Data Reduction
- 3. Screening and Correcting for Halogen Degassing and Alteration
- 4. Measured Compositions of Reykjanes Ridge Basalts
- 5. Reverse Fractional Crystallization
- 6. Calculating the Halogen Contents of Enriched and Depleted Mantle Endmembers
- 7. Literature Datasets: Reykjanes Ridge, Atlantic and Global MORB
- Tables S-1 to S-9
- Figures S-1 to S-12
- Supplementary Information References

1. Sample Collection

The samples investigated in this study were dredged from the Reykjanes Ridge between 57.7 and 63°N, at radial distances of ~1000 to ~400 km from the Iceland plume centre (Fig. S-1). All samples were collected during the RSS Charles Darwin cruise CD80 as part of the PETROS sampling programme (Murton, 1995). The samples comprise quenched basaltic glass from pillows or sheet flows, and from two seamounts towards the southwest end of the ridge segment. Previous studies have reported elemental, isotopic and redox geochemistry in these samples (Hilton *et al.*, 2000; Murton *et al.*, 2002; Nichols *et al.*, 2002; Shorttle *et al.*, 2015; Novella *et al.*, 2020; Hartley *et al.*, 2021; Balci *et al.*, 2026).

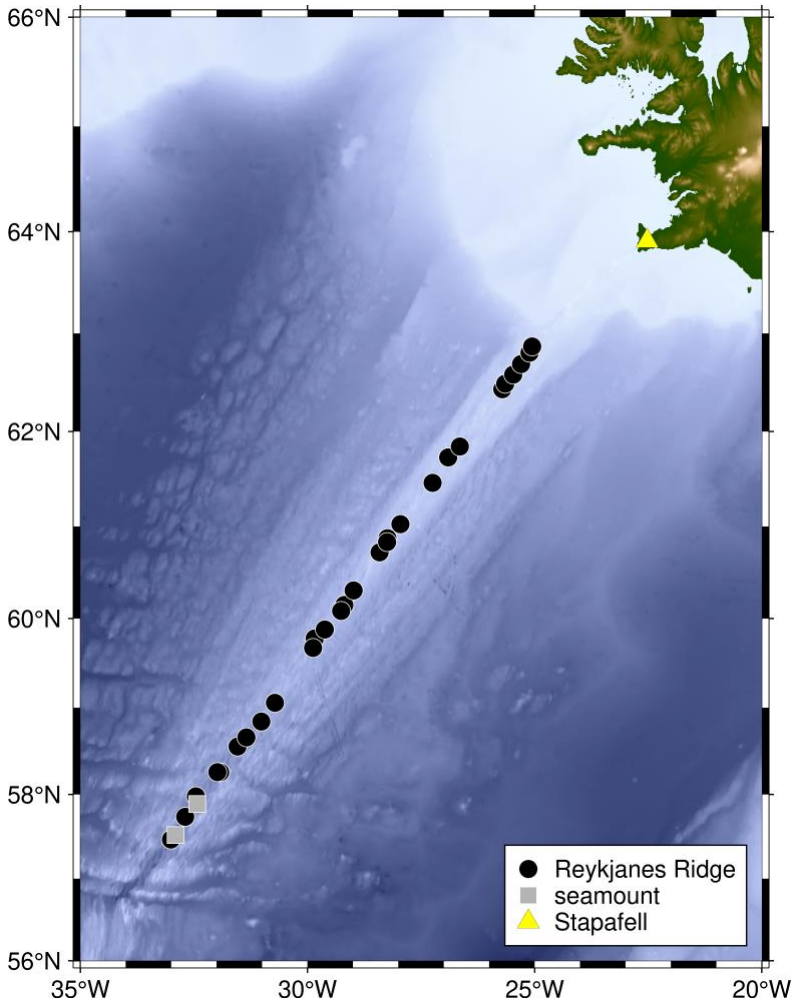


Figure S-1 Map showing the locations of dredged basalt samples from the Reykjanes Ridge investigated in this study. The locations of two seamounts are shown as grey squares. The location of Stapafell on the Reykjanes Peninsula of Iceland is shown as a yellow triangle.

2. Analytical Methods and Data Reduction

Analysis of heavy halogens

The Cl, Br and I contents of basaltic glass samples from the Reykjanes Ridge were measured by neutron irradiation noble gas mass spectrometry (NI-NGMS) at the University of Manchester. Our sample preparation, irradiation, analysis protocol and data reduction approaches are described in detail by Ruzié-Hamilton *et al.* (2016).

NI-NGMS determination of halogen contents in geological samples is based on an extension of the ^{40}Ar-^{39}Ar technique (Kendrick, 2012, and references therein). Neutron-induced reactions convert parent halogen, K and Ca isotopes to daughter noble gas isotopes that are either stable or have relatively long half-lives (e.g., $^{37}Ar_{Ca}$ t½ = 37.1 d; $^{39}Ar_{K}$ t½ = 269 yr). The daughter isotopes are used as proxies to determine the concentration of the halogens, K and Ca. Standards with known halogen contents are irradiated and analysed alongside the unknowns in order to derive the correction factors required for data reduction (Ruzié-Hamilton *et al.,* 2016).

Sample irradiation

For each sample, glass chips 1-3 mm in size were examined under a binocular microscope to select those that were fresh, unaltered and free from visible crystals or inclusions. Selected chips were cleaned in an ultrasonic bath with deionised water, acetone, 5% nitric acid, and a final wash in deionised water to ensure removal of any surface contamination.

Approximately 30 mg of each clean sample was weighed out and wrapped in aluminium foil. Packaged samples were stacked into 6.5 cm (length) × 0.8 cm (outer diameter) fused silica tubes and interspersed every approx. 2 cm with irradiation standards Hb3gr hornblende (Turner *et al.*, 1971), scapolites BB1 and BB2 (Kendrick, 2012), and pyroxene grains hand-picked from the Shallowater aubrite meteorite (Gilmour *et al.*, 2006). Standards were used to monitor vertical neutron fluence variations and neutron-induced noble gas production rates within each silica tube. Hb3gr was placed at the top, middle and bottom of the tube; scapolites at the top and bottom; and Shallowater in the centre of the tube. Following sample loading, tubes were flame-sealed under vacuum.

The samples were irradiated in two batches using separate irradiation facilities. The majority of samples (n=26) were irradiated at the in-core irradiation tube (ICIT) facility, Oregon State University (OSU) TRIGA reactor. The irradiation (designated MN2019) was carried out over a period of two months between 9 December 2019 and 10 February 2020 in a series of time steps with a cumulative irradiation time of 200 hours. Corrections factors for radioactive decay of ^{37}Ar and ^{39}Ar decay were determined using equations of Wijbrans (1985) for multi-step irradiations. The remaining samples (n=7) were irradiated continuously for 24 hr at the High Flux Reactor, Petten, Netherlands (irradiation MN2012b; see Ruzié-Hamilton *et al*., 2016, for further details). Following irradiation, samples were unpacked from tubes and standards were analysed to determine irradiation parameters.

Neutron Irradiation Noble Gas Mass Spectrometry (NI-NGMS)

For samples irradiated in MN2012b, approximately 25 mg of each sample was analysed by heating in a resistance furnace over three temperature steps (600-1400-1600 °C), each of 30 min duration. During heating, gases released from the sample were purified using a SAES GP50 getter at 450 °C. Following clean-up, noble gases were cryogenically transferred to the inlet of the MS1 mass spectrometer for isotopic analysis (Ruzié-Hamilton *et al.,* 2016). For samples irradiated in MN2019, aliquots of between 2-8 mg were loaded into 3 mm diameter holes drilled into an Al sample holder. The sample holder was placed in the laser port chamber connected to a noble gas preparation line and baked at 120 °C for 12 hours while pumping down to ultra-high vacuum. A 55 W CO_2 laser (λ = 10.6 μm) was used to fuse the samples for 2 min using 12% output power and a beam diameter of 3 mm. This was followed by a further 3 min gas purification using two SAES NP10 getters, one held at 450 °C and the other at room temperature. Following the 5 min

extraction and purification step, noble gases were admitted to a ThermoFisher ARGUS VI mass spectrometer. Isotopic analysis using the ARGUS VI and MS1 mass spectrometers followed similar procedures where ion intensities of m/z corresponding to Ar, Kr and Xe isotopes were determined using peak hopping by switching the magnetic field. At the end of the analysis, the amounts of each isotope were obtained by regression of the ion beam intensities to mass spectrometer inlet time. Blank levels on the ARGUS VI experiments were determined at the start of each day, and after every fourth sample analysis, using an identical procedure to samples but without laser heating. Blanks were consistent within 20% and average values are 2.29×10^{-13} cm^3 STP ^{38}Ar, 1.48×10^{-14} cm^3 STP ^{80}Kr, and 2.70×10^{-15} cm^3 STP ^{128}Xe; in all cases, blank levels represent <1% of the typical sample release of halogen-derived noble gas isotopes. Blanks for the MS1 samples were determined on an empty furnace tube to be 4.9×10^{-10} cm^3 STP ^{40}Ar, 4.4×10^{-14} cm^3 STP ^{84}Kr, and 5.5×10^{-15} cm^3 STP ^{132}Xe with an approximately atmospheric isotopic composition. Irradiation standards Hb3gr, BB1, BB2 and Shallowater from each irradiation were loaded and analysed using the same protocol as the samples. The sensitivity and mass discrimination of the MS1 and ARGUS VI mass spectrometers were determined daily by measuring aliquots of air from a bottle of known pressure.

Data reduction and irradiation standards

Noble gas data were corrected for blanks, Ar, mass discrimination, ^{37}Ar and ^{39}Ar decay and neutron interference corrections. Irradiation parameters and noble gas conversion ratios (cm^3 STP/g) were determined from the standards using the expressions shown in Table S-1 and their values are given in Table S-8 (provided as an Excel data sheet). Following minor correction for atmospheric noble gases based on quantities of ^{36}Ar, ^{84}Kr and ^{129}Xe and assuming air ratios, the irradiation parameters were used to convert daughter noble gas isotopes to parent element concentrations. In accordance with the recommendations of Ruzié-Hamilton *et al.* (2016) we have used scapolite-corrected ^{79}Br values for our Reykjanes Ridge unknowns. We also use scapolite-corrected I values, since this yields a lower propagated analytical uncertainty.

Assessment of sample homogeneity

Duplicate measurements on each Reykjanes Ridge sample in irradiation MN2019 were made using separate 2-8 mg aliquots to assess the compositional heterogeneity of each unknown. In nine cases, one or more of the Cl, Br, I measurements differed by more than the 2σ analytical uncertainty, and so a third 2-8 mg aliquot was analysed. Chlorine, Br and K measured in separate aliquots of the same sample lie close to the 1:1 correlation (Fig. S-2), and we take the mean Cl, Br and K measurements as representative of the bulk sample.

There is considerable variability in the I contents measured in different aliquots of the same sample (Fig. S-2c), despite homogenous Cl, Br, K contents in these same aliquots. We infer that there is a degree of heterogeneity in the I contents of different glass chips from the same sample. High I/Cl accompanied by mantle-like Br/Cl is indicative of low-temperature oxidised alteration fixing seawater iodate (Kendrick *et al.*, 2017; Kendrick, 2019). Sample aliquots with unusually high I/Cl compared to typical depleted MORB mantle (red points in Fig. S-3a) are therefore considered to contain material that has undergone alteration; these measurements are not considered further. From the filtered dataset, we then compare the mean and lowest iodine measurements for each sample (Fig. S-3b). We find a strong positive correlation between the mean Cl content and the lowest I content (r^2=0.74), whereas the correlation between mean Cl and mean I is more widely scattered (r^2=0.44). We consider that the lowest measured I contents provide the best representation of melt I content, ensuring that our dataset is minimally affected by I addition through seawater alteration.

Table S-1 Irradiation parameters and standards used for conversion of noble gas isotopes to parent element abundances in neutron-irradiated samples. The general expressions can be related directly to any standard with independently determined K, Cl, Br and I compositions.

Parameter[a]	General expression[b]	Standard[c]
J	$J = \frac{(e^{\lambda t} - 1)}{(^{40}Ar / {}^{39}Ar_K)}$	Hb3gr
$^{39}Ar_K/K$	$\left(\frac{^{39}Ar_K}{K}\right) = J \cdot \left(\frac{^{40}K}{K}\right) \cdot \left(\frac{\lambda_e}{\lambda}\right) = 7.0124 \times 10^{-3} \cdot J$	Hb3gr
β	$\beta = \left(\frac{K}{Cl}\right) \cdot \left(\frac{^{38}Ar_{Cl}}{^{39}Ar_K}\right)$	Hb3gr
$^{38}Ar_{Cl}/Cl$	$\left(\frac{^{38}Ar_{Cl}}{Cl}\right) = 7.0124 \times 10^{-3} \cdot J \cdot \beta$	Hb3gr
π	$\pi = \left(\frac{Cl}{Br}\right) \cdot \left(\frac{^{80}Kr_{Br}}{^{38}Ar_{Cl}}\right)$	Scapolite
$^{80}Kr_{Br}/Br$	$\left(\frac{^{80}Kr_{Br}}{Br}\right) = 7.0124 \times 10^{-3} \cdot J \cdot \beta \cdot \pi$	Scapolite
ω	$\omega = \left(\frac{Cl}{I}\right) \cdot \left(\frac{^{128}Xe_I}{^{38}Ar_{Cl}}\right)$	Scapolite
$^{128}Xe_I/I$	$\left(\frac{^{128}Xe_I}{I}\right) = 7.0124 \times 10^{-3} \cdot J \cdot \beta \cdot \omega$	Scapolite
$^{128}Xe_I/I$	$\left(\frac{^{128}Xe_I}{I}\right) = \left(\frac{^{129}Xe}{I}\right)_0 \cdot \left(\frac{^{128}Xe_I}{^{129}Xe}\right)$	Shallowater

[a] ^{40}K decay constants for electron capture $\lambda_e = 0.581 \times 10^{-10}$ yr^{-1} and total decay $\lambda = 5.463 \times 10^{-10}$ yr^{-1} (Steiger and Jäger, 1977). $^{40}K/K = 0.01167$.

[b] Noble gas/parent element ratios (e.g. $^{38}Ar_{Cl}/Cl$) are in units of cm^3 STP/g.

[c] Hb3gr is a hornblende monitor used in ^{40}Ar-^{39}Ar dating with K = 1.247 ± 0.008 wt.% and Cl = 0.283±0.002 wt.% (Roddick, 1983). The age *t* of this monitor is 1081.0±1.2 Ma (Renne *et al.*, 2011). BB1 scapolite has Cl = 3.08±0.13 wt.% and Br = 430±30 µg/g (Kendrick *et al.*, 2013). The initial $(^{129}Xe/I)_0$ of the Shallowater meteorite is $(1.072 \pm 0.029) \times 10^{-4}$ (Brazzle *et al.*, 1999).

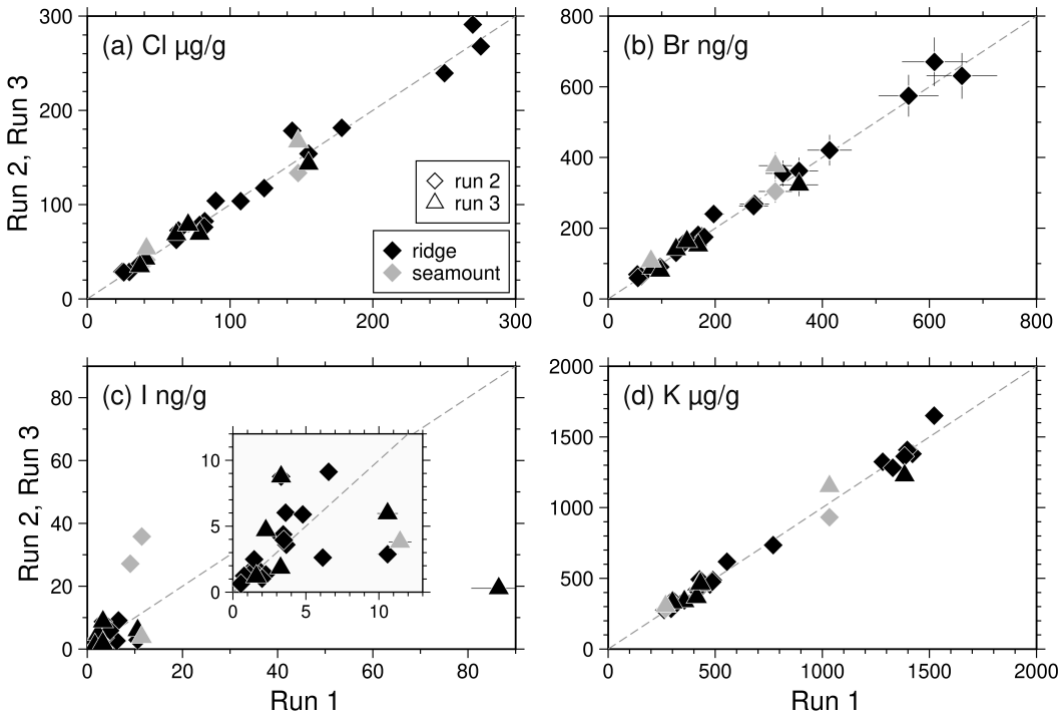


Figure S-2 Comparison of repeat analyses of Cl, Br, I and K in Reykjanes Ridge basalts, measured in separate 2-8 mg aliquots from the same sample. Diamond symbols compare the measurements made on aliquots 1 and 2. Triangles compare measurements made on aliquots 1 and 3 (nine samples). Grey dashed line shows 1:1 correlation. Error bars are 1σ and are mostly smaller than symbol size.

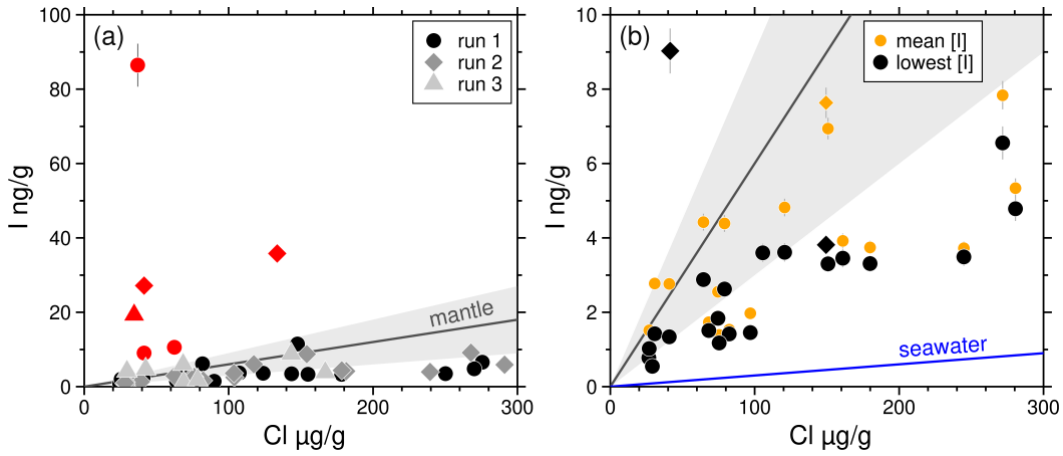


Figure S-3 **(a)** Variability in I and Cl contents measured in different aliquots of Reykjanes Ridge basalt samples. Error bars are 1σ and are mostly smaller than symbol size. Grey solid line and shaded region indicate the preferred mantle I/Cl of $(60\pm30)\times10^{-6}$, from Kendrick *et al.* (2017). Red symbols indicate aliquots with unusually high I/Cl, indicative of low-temperature seawater alteration. **(b)** Mean (orange) and lowest (black) I contents for each sample, plotted against the mean Cl value of the sample. Diamond symbol indicates seamount 14D4. Seawater I/Cl of 3×10^{-6} is shown for reference.

3. Screening and Correcting for Halogen Degassing and Alteration

From a mantle geochemical perspective, it is important to ascertain whether the measured halogen contents have been modified by magma degassing or by assimilation of seawater or brines. The Reykjanes Ridge is unusual in its lack of hydrothermal centres: shipboard surveys of the Reykjanes Ridge between 57.6°N and 63.2°N have detected only one hydrothermally active site, the Steinahóll vent field at 63.1°N (German *et al.*, 1994). Although this site is located ~40 km along the ridge from our most northerly sample (62.87°N), seawater assimilation could feasibly increase with proximity to the active hydrothermal site. Simultaneously, as the Reykjanes Ridge shallows towards Iceland, samples are erupted under progressively lower hydrostatic confining pressures. Submarine basalts erupted into water depths >500 m have been proposed to remain halogen-undersaturated due to the effect of hydrostatic pressure (Unni and Schilling, 1978). Five of our samples were erupted north of 62.6°N into water depths ≤500 m. If these samples were affected by syn-eruptive degassing, then the extent of halogen enrichment towards Iceland and/or the effects of any seawater assimilation may be masked.

We observe a three-fold increase in measured halogen contents in basalts erupted north of 62°N into water depths ≤550 m, as the ridge shallows towards Iceland (Fig. S-4). To test whether the halogen contents of the Reykjanes Ridge samples are pristine or modified, we compared glass halogen contents against La, an incompatible trace element that exhibits similar partitioning behaviour to the halogens during crystallization of volatile-undersaturated melt. Although La is slightly more compatible in basaltic melts than Cl or Br (Schilling *et al.*, 1980), all these elements are highly incompatible in the silicate phases likely to crystallize from basaltic melts. Thus, Cl/La, Br/La and I/La are all expected to remain constant during crystallization of halogen-undersaturated melt. This means that La can be used as a proxy for the undegassed halogen content of melts, if the primary melt halogen/La ratios are known.

We have estimated primary halogen/La ratios for the Reykjanes Ridge using the best-fit linear regression defined by 23 samples erupted into water ≥600 depth (Fig. S-5), a confining pressure at or above which halogens are expected to remain undersaturated (Unni and Schilling, 1978). The best-fit ratios define unmodified halogen/La ratios for the Reykjanes Ridge basalts of Cl/La = 42.0, Br/La = 97.1×10^{-3} and I/La = 1.12×10^{-3} (Fig. S-5). Our Reykjanes Ridge Cl/La is somewhat higher than the mean Cl/La of 21.8±13.3 (1σ) for unaltered Atlantic MORB; Br/La falls within the Atlantic MORB range of $(58.6\pm37.1)\times10^{-3}$, and I/La precisely matches the mean Atlantic MORB value of $(1.12\pm0.67)\times10^{-3}$ (Kendrick *et al.*, 2017).

The predicted undegassed halogen content of a glass (*pr*) can be calculated from its measured La content (La^{gl}) and the halogen/La ratio of the initial primary melt (*ini*) is known:

$$hal^{pr} = La^{gl}\left[\frac{hal}{La}\right]_{ini}$$

For six Reykjanes Ridge glasses erupted into water ≤550 m deep, we used measured La contents (Novella *et al.*, 2020) in conjunction with the unmodified halogen/La ratios to calculate estimates of their undegassed halogen contents. In all cases the predicted undegassed halogen contents are higher than those measured by NI-NGMS. A degassing correction was applied if the difference between measured and predicted halogen content exceeded 2σ analytical uncertainty. Three samples were corrected for Cl, Br and I degassing, and two samples were corrected for I degassing only (Fig. S-5).

None of the six samples most proximal to the Steinahóll hydrothermal site have elevated halogen/La ratios that would indicate seawater assimilation. However, five samples distributed randomly along the ridge segment have high I contents coupled with I/La exceeding 1.8×10^{-3}, but no corresponding enrichment in Br or Cl. Mean Reykjanes Ridge Br/Cl=$(2.3\pm0.2)\times10^{-3}$ falls comfortably within the global mantle range of $(2.8\pm0.8)\times10^{-3}$ (Fig. 1b), indicating no assimilation of saline brines. High I/Cl accompanied by mantle-like Br/Cl is likely indicative of either low-temperature oxidised seawater alteration (e.g., Kendrick, 2019) or introduction of biophilic I through microbial alteration (Templeton *et al.*, 2005). Measured La contents were used as a proxy to restore the I contents of the five altered samples.

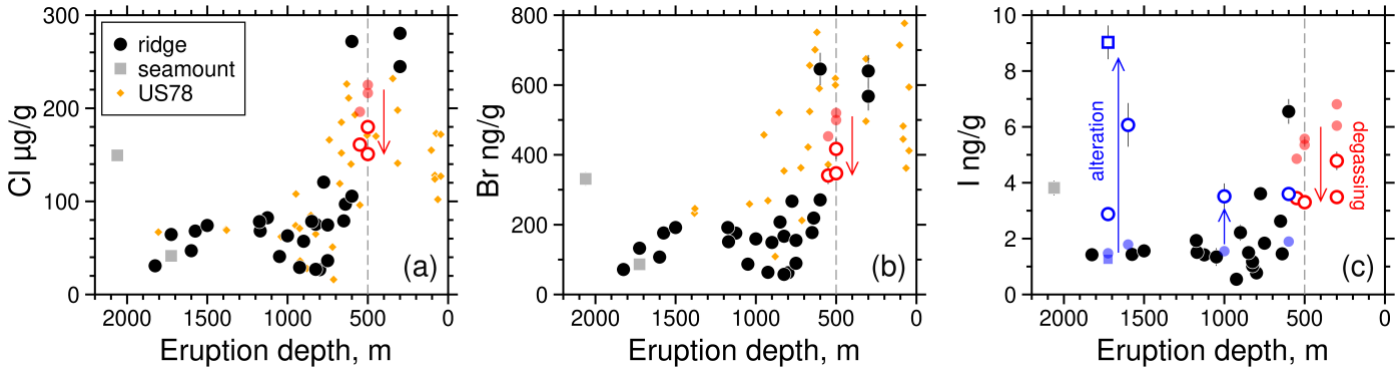


Figure S-4 Reykjanes Ridge glass **(a)** Cl, **(b)** Br and **(c)** I contents vs water depth. Error bars are 1σ and are mostly smaller than symbol size. Large symbols indicate measured halogen concentrations. Dashed vertical lines show the critical depth of degassing proposed by Unni and Schilling (1978) for Cl and Br. We find no correlation between water depth and halogen content for water depths ≥600 m, indicating these samples are halogen undersaturated and undegassed. Red open symbols are samples interpreted to have degassed halogens. Blue open symbols are samples interpreted to have gained I via seawater or microbial alteration. Small pale circles show corrected halogen contents for the degassed and altered samples. Orange diamonds are Reykjanes Ridge whole rocks (Unni and Schilling, 1978); note that samples erupted into water depth <500 m show low and variable Cl and Br contents, suggestive of degassing.

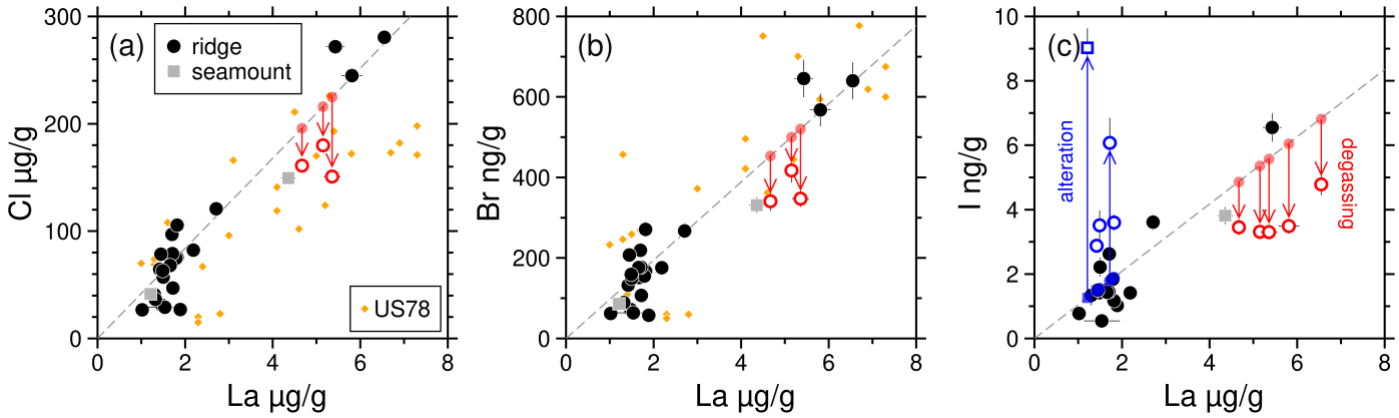


Figure S-5 Reykjanes Ridge glass **(a)** Cl, **(b)** Br and **(c)** I contents vs La. Error bars are 1σ and are mostly smaller than symbol size. Dashed lines show best-fit halogen/La ratios for samples erupted into water depths of ≥600 m, which are assumed to be pristine and undegassed. Red open symbols indicate samples erupted into water <550 m deep with measured halogen/La ratios significantly lower than the best-fit correlation, indicative of halogen degassing. Blue open symbols indicate samples with measured I/La significantly higher than the best-fit correlation, indicative of I gain via seawater or microbial alteration. Halogen contents are corrected for degassing and alteration by restoring to the best-fit halogen/La ratio, shown by the pale coloured circles. Orange diamonds are Reykjanes Ridge whole rocks (Unni and Schilling, 1978). Five of the six samples with La >4.5 µg/g were erupted into water depths <550 m; all appear to have partially degassed I, and three have also partially degassed Cl and Br.

4. Measured Compositions of Reykjanes Ridge Basalts

Following corrections for degassing or alteration, Reykjanes Ridge basalts contain 27-281 µg/g Cl, 57-646 ng/g Br and 0.5-6.8 ng.g I (Fig. 1, Fig. S-6). These glass compositions show along-ridge increases in Cl, Br and I contents north of 61°N (Fig. S-7). Our measured Cl contents are similar to those measured in a different suite of 36 Reykjanes Ridge basalts from between 57.6°N and 63.6°N (Unni and Schilling, 1978), which includes 7 samples from within 0.2° of the Steinahóll hydrothermal field at 63.1°N. Both sample suites show decreases in measured Cl contents north of 62.4°N where the water depth shallows to <500 m, indicating that these samples have degassed a portion of their original Cl contents (Fig. S-7a; note that the Unni and Schilling, 1978, samples have not been corrected for degassing or alteration in this figure). Our measured Br contents are on average lower and less variable than those reported by Unni and Schilling (1978) (Fig. S-7c). Consequently, we recover lower and less variable Br/Cl (Fig. S-6b) that remains constant along the ridge segment (Fig. 2 of main text). Our Cl/K and Br/K ratios are likewise less variable than those previously reported (Fig. 2 of main text). Our halogen/K ratios are calculated from halogen and K measurements made in the same glass chips by the same technique (NI-NGMS). In contrast, the literature halogen and K data were measured in different aliquots of the same samples and by different techniques – halogens by whole-rock instrumental neutron activation analysis (INAA; Unni, 1976) and K_2O by wet chemistry (Schilling *et al.,* 1983) – which may contribute additional noise to the along-ridge halogen/K ratios.

Once corrected for degassing or alteration, our samples from the northern Reykjanes Ridge ≥61°N are progressively enriched in halogens approaching Iceland and show minor along-ridge increases in halogen/K ratios, but Br/Cl and I/Cl do not show systematic along-ridge variability. The southern ridge sector <61°N has far less variable halogen abundances: the observed minor variability in Cl and Br contents is of the order of the 1σ standard deviation for the southern ridge sector (Fig. S-7).

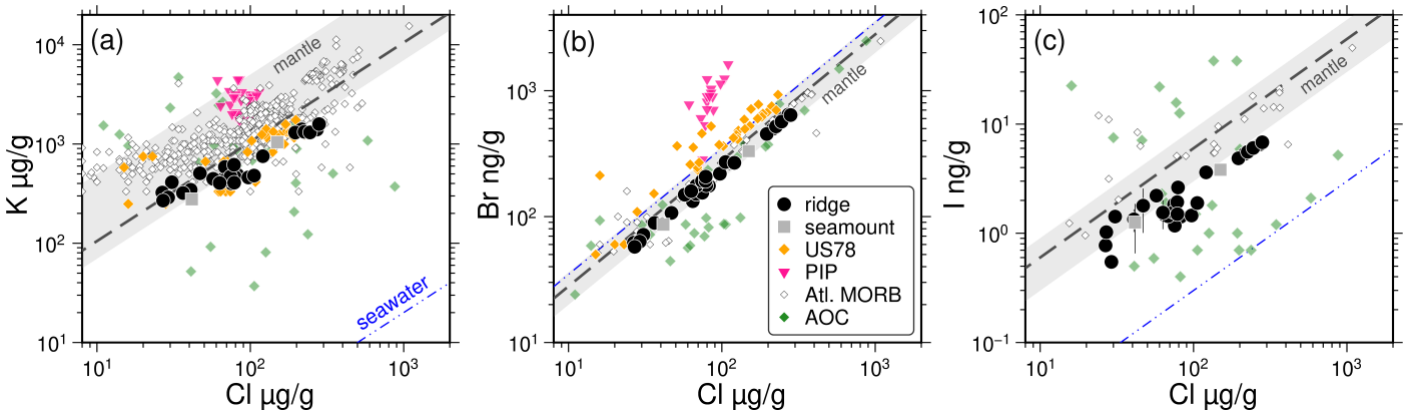


Figure S-6 Halogen and K contents of Reykjanes Ridge glasses measured by NI-NGMS, and after correction for degassing or alteration: **(a)** K vs Cl; **(b)** Br vs Cl; **(c)** I vs Cl. Red and blue open symbols show glass compositions before correction for degassing (red) or alteration (blue). Error bars are smaller than symbol size. Dashed lines and shaded bars show mantle K/Cl, Br/Cl and I/Cl ratios and their 1σ ranges (Kendrick *et al.*, 2017). Dashed blue line shows the composition of seawater (Li, 1991). Orange diamonds are Reykjanes Ridge whole rocks (US78; Unni and Schilling, 1978). Pink triangles are olivine-hosted melt inclusions in proto-Iceland plume basalts from Baffin Island and West Greenland (PIP; Tomlinson *et al.*, 2025). Atlantic MORB compositions compiled from PetDB (Atl. MORB; www.earthchem.org/petdb). Green diamonds show hydrothermally altered oceanic crust (AOC; Chavrit *et al.*, 2016).

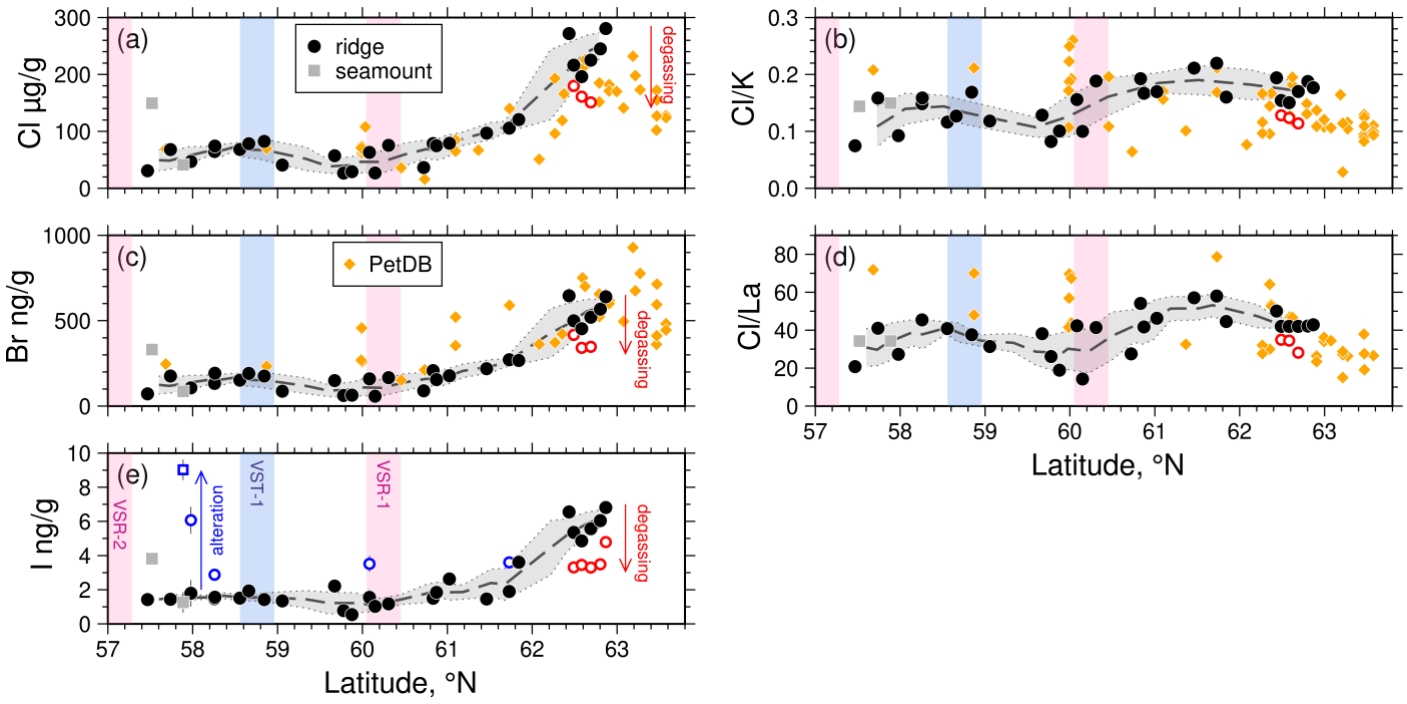


Figure S-7 Along-ridge compositional variation in Reykjanes Ridge glasses. **(a, c, e)** halogen contents, shown without correction for fractional crystallization; **(b)** Cl/K and **(d)** Cl/La. Error bars are 1σ and in many cases are smaller than the symbol size. Vertical bands show where V-shaped ridges (VSR, pink) and troughs (VST, blue) intersect the ridge axis (Jones *et al.*, 2014). Red and blue open symbols show measured halogen contents without correction for degassing (red) or alteration (blue). Dashed lines and shaded areas show the along-ridge running average and 1σ standard deviation, calculated using a boxcar filter with bandwidth of 2 degrees latitude. Orange diamonds are Reykjanes Ridge whole rocks (Unni and Schilling, 1978) compiled from PetDB, and are shown without correction for fractional crystallization, degassing or alteration. Equivalent plots of halogen concentrations after applying a fractional crystallization correction to 10 wt.% MgO are shown in Figure 3e,g,i of the main text.

Table S-2 Data sources plotted and/or used to generate the compositional fields shown in Figure 3 of the main text.

Symbol or field		Reference
Dark pink inverted triangles	Proto-Iceland plume basalt glasses from Baffin Island	Kendrick *et al*. (2015b)
Pink inverted triangles	Olivine-hosted melt inclusions in proto-Iceland plume basalts from Baffin Island	Tomlinson *et al*. (2025)
Purple triangles	Glasses from Kama‘ehuakanaloa Seamount (i.e., Lō‘ihi)	Kendrick *et al*. (2025)
Pink pentagons	Global OIB: Pitcairn, Society, Samoa, Hawai‘i	Kendrick *et al*. (2017, 2025)
Grey circles	Global MORB	Compiled from PetDB
Open diamonds	Atlantic MORB	Compiled from PetDB
Blue diamonds	Altered MORB	Kendrick *et al*. (2017)
Green diamonds	Low- and high-temperature altered oceanic crust	Chavrit *et al*. (2016)
Blue star	Seawater	Li (1991)
Blue fields	Brine compositions	Kendrick *et al*. (2015a)
Grey fields	Mantle range	Kendrick *et al*. (2017)
	Reykjanes Ridge glass H_2O contents, panel (c)	Nichols *et al*. (2002)

5. Reverse Fractional Crystallization

Fractional crystallization generates significant variability in the halogen contents of Reykjanes Ridge glasses erupted north of 61°N. To explore mantle-derived variability in primary melt halogen contents, we used Petrolog 3.1.1.3 (Danyushevsky and Plechov, 2011) to calculate reverse fractional crystallization corrections to restore melt compositions to 10 wt.% MgO. Starting compositions were the glass major element compositions reported by Shorttle *et al.* (2015), apart from two samples for which only bulk-rock compositions were available (50D3G and 66D3; Murton *et al.,* 2002). We assume that the melts are anhydrous. To ensure comparability between this and previous studies, we follow the approach of Shorttle *et al.* (2015): major elements are first corrected for fractionation of olivine + plagioclase + clinopyroxene until melt compositions reach 8 wt.% MgO, and further correction proceeds assuming only olivine as a liquidus phase. Calculation outputs were extracted when the melt reached 10 wt.% MgO, and again when the melt reached equilibrium with Fo_{90} olivine. Mineral-melt equilibrium models were Herzberg and O'Hara (2002) with Kd_{Fe-Mg}^{ol-liq} after Toplis (2005) for olivine, and Danyushevsky (2001) for clinopyroxene and plagioclase. All calculations were run at 1.5 kbar pressure with oxygen fugacity at 0.3 log units above the quartz-fayalite-magnetite (QFM) buffer.

Experimentally determined partition coefficients were used to calculate the effect of reverse fractional crystallization on melt K contents (Table S-3). We tested the assumption of perfect Cl incompatibility in silicate minerals versus applying an experimentally determined olivine-melt partition coefficient (Joachim *et al.*, 2015; Table S-3). The difference between these approaches is on the same order as, or less than, the 1σ analytical uncertainty of our NI-NGMS measurements. For simplicity, we assume that Cl, Br and I are perfectly incompatible in all phases.

Atlantic and global MORB compositions compiled from PetDB were corrected for reverse fractional crystallization following the same procedure as the Reykjanes Ridge glasses, but with oxygen fugacity set to 0.1 units above the QFM buffer, appropriate for global MORB (Berry and O'Neill, 2021).

Table S-3 Mineral-melt partition coefficients for K and Cl used in reverse fractional crystallization calculations. [a]Philpotts and Schnetzler (1970); [b]Aigner-Torres *et al.* (2007); [c]Hart and Dunn (1993); [d]Joachim *et al.* (2017).

Element i	$D_i^{ol-melt}$	$D_i^{plag-melt}$	$D_i^{cpx-melt}$
K	0.0056[a]	0.22[b]	0.0072[c]
Cl	0.00022[d]	-	-

Fractionation-corrected compositions of Reykjanes Ridge basalts

Reykjanes Ridge glasses required 3-42% (mean 15%) fractional crystallization correction to restore their compositions to 10 wt.% MgO. After fractionation correction, the Reykjanes Ridge basalts contain 20-190 µg/g Cl, 43-439 ng/g Br and 0.5-4.7 ng/g I. Halogen/halogen ratios are not affected by the fractionation correction, since all halogens are assumed to be perfectly incompatible in all phases. Fractionation-corrected halogen/K ratios are lower than measured halogen/K ratios; the difference is of the same order as the 1σ analytical uncertainty. Primary melt Cl, Br and I abundances correlate positively with lithophile isotopes; trace element concentrations; and Nb/Zr, a ratio of two similarly incompatible trace elements that are not fractionated from one another during mantle melting or magma crystallization; but show no correlation with $^3He/^4He$ (Fig. S-8). Fractionation-corrected halogen/K ratios show no systematic relationship with lithophile isotopes, Nb/Zr, or $^3He/^4He$ (Fig. S-8, S-9).

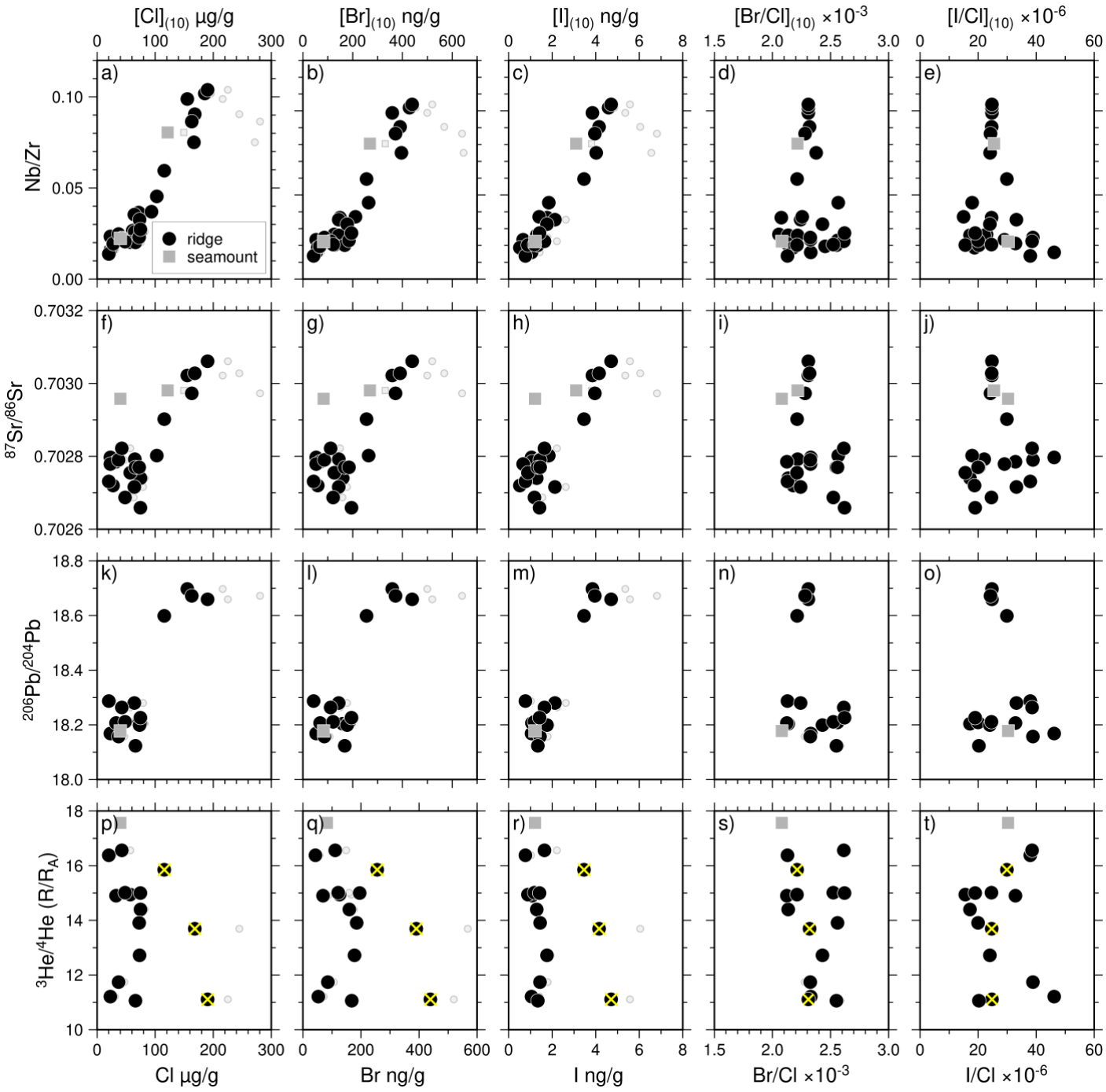


Figure S-8 Reykjanes Ridge basalt halogen contents, Br/Cl and I/Cl ratios versus **(a–e)** Nb/Zr, a ratio of two similarly incompatible trace elements; **(f–o)** Sr and Pb lithophile isotope ratios; **(p–t)** He isotope ratios. Large symbols show compositions after fractionation correction to 10 wt.% MgO. Small open symbols show the same samples without correction for fractional crystallization. Yellow crosses in **(p–t)** are samples from ≥61°N that have been suggested to be affected by degassing and addition of radiogenic helium upon mantle-crust interactions (Hilton *et al*., 2000). Halogen contents correlate positively with Nb/Zr and lithophile isotope ratios. We find no systematic correlation between halogen contents and helium isotopic signature, nor between halogen ratios and any trace element or isotopic indicator of geochemical enrichment. Trace element data from Murton *et al*. (2002); Sr and Pb isotope data from Hilton *et al.* (2000), Murton *et al.* (2002) and Thirlwall *et al.* (2004); He isotope data from Hilton *et al.* (2000).

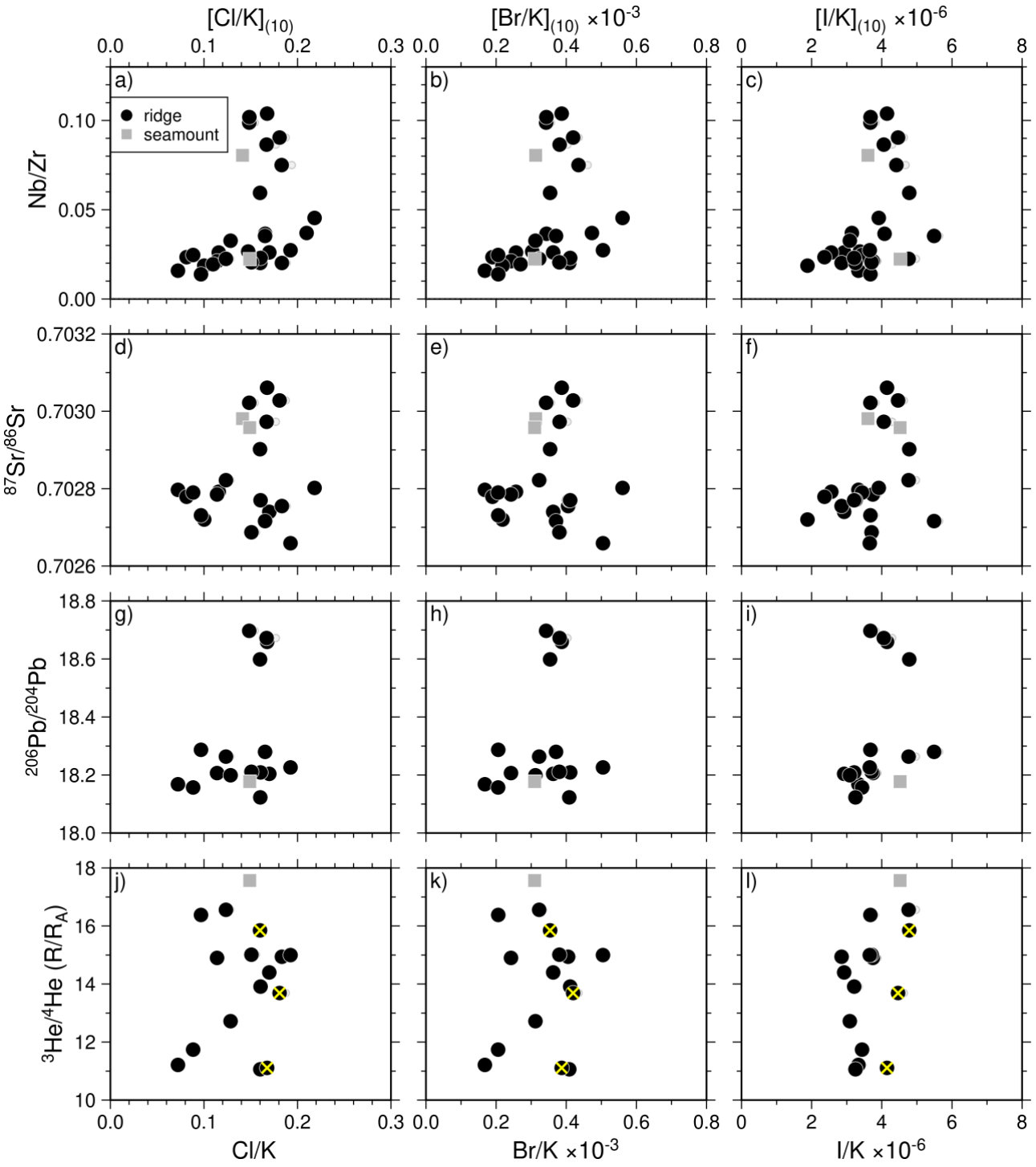


Figure S-9 Reykjanes Ridge halogen/K ratios versus **(a–c)** a ratio of two similarly incompatible trace elements Nb/Zr; **(d–i)** Sr and Pb lithophile isotope ratios; **(j–l)** He isotope ratios. Legend, symbols and data sources as for Figure S-8. Halogen/K ratios show no systematic relationship with trace element or isotopic indicators of geochemical enrichment.

6. Calculating the Halogen Contents of Depleted and Enriched Mantle Endmembers

Partial melting model

We constructed a simple melting model to estimate the mantle lithology, composition and melting degree required to produce the observed compositions of our Reykjanes Ridge samples, and for the Stapafell basalts on Iceland's Reykjanes Peninsula. We consider the following starting mantle lithologies:

1) spinel lherzolite, sp_2:ol_{55}:opx_{25}:cpx_{18} (spinel:olivine:orthopyroxene:clinopyroxene);
2) spinel pyroxenite, sp_7:ol_{18}:opx_{15}:cpx_{60};
3) garnet lherzolite, gt_{20}:ol_{54}:opx_{17}:cpx_9 (gt = garnet);
4) garnet pyroxenite, gt_{27}:ol_{23}:cpx_{50}.

Mantle lithologies (1), (2) and (4) are the same as those used by Shorttle *et al.* (2015) in melting models to estimate plausible source Fe_2O_3 contents for enriched and depleted mantle lithologies beneath Iceland and the Reykjanes Ridge. For each mantle type, melting calculations were performed assuming a depleted MORB mantle (DMM) starting composition (La = 0.192 µg/g, Y = 3.328 µg/g, Zr = 5.082 µg/g; Workman and Hart, 2005) and a primitive mantle (PM) composition (La = 0.6832 µg/g, Y = 4.13 µg/g, Zr = 10.3 µg/g; Palme and O'Neill, 2014). We also modelled melting of the KG-1 pyroxenite composition proposed by Novella *et al*. (2020; La = 0.96 µg/g, Y = 16.31 µg/g, Zr = 35.75 µg/g), which they calculated by mixing depleted peridotite from Salters and Stracke (2004) with recycled oceanic crust from Stracke *et al*. (2003). Melting models were calculated using the aggregate fractional melt equation:

$$C_l = C_s \left(\frac{1}{F\left(1 - (1-F)^{\left(\frac{1}{D}\right)}\right)} \right)$$

where C_l is the liquid composition, C_s is the solid composition, F is the melt fraction, and D is the bulk partition coefficient. Trace element mineral-melt partition coefficients were taken from Brown and Lesher (2016).

The trace element contents and ratios in Reykjanes Ridge glasses south of 61°N are best modelled by 8-13% partial melting of depleted spinel peridotite, consistent with previous studies (Murton *et al.*, 2002). Glasses north of 61°N lie on the depleted spinel peridotite melting curve at melting degrees of 2-6% (Fig. S-10). However, lower melting degrees are not consistent with the increasing crustal thickness towards Iceland. The more enriched trace element signatures approaching Iceland are better explained by mixing melts of depleted spinel peridotite with melts derived from more enriched mantle and/or low-degree melts derived from garnet-bearing mantle (Fig. S-10).

Our simple model suggests that the La-Zr-Y systematics of Stapafell basalts from the Reykjanes Peninsula of Iceland can be matched by ~12% melting of spinel pyroxenite with PM-like composition (Fig. S-10). However, major element systematics of Icelandic basalts are inconsistent with melting a single source lithology (Shorttle and Maclennan, 2011), and more complex melting models indicate that Stapafell magmas are aggregates of instantaneous melts derived from both garnet- and spinel-facies mantle. For example, Novella *et al*. (2020) proposed that low-degree (4-10%) melting of the KG1-like pyroxenite, with melting taking place in both garnet and spinel stability fields, can reproduce some of the trace element characteristics of Stapafell basalts. While our model suggests that melting of a KG1-like pyroxenite cannot explain the La-Zr-Y systematics of Stapafell, it does support the interpretation that Stapafell-like melts can be generated as mixtures of melts derived from a depleted spinel peridotite with melts derived from an enriched garnet lherzolite or garnet pyroxenite.

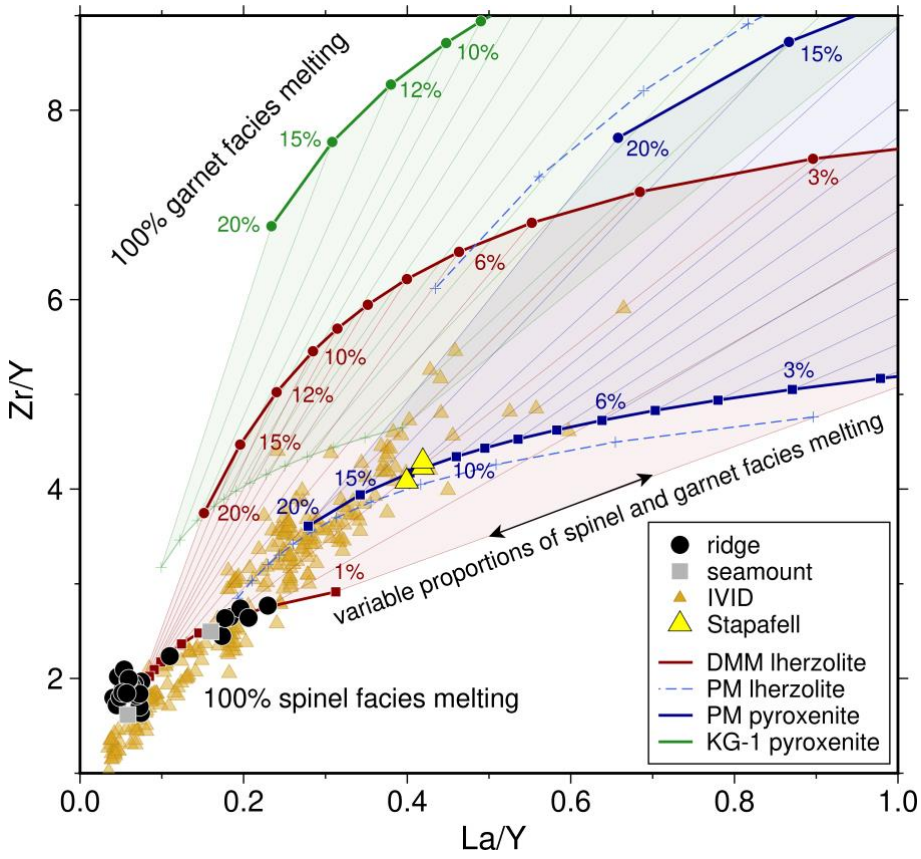


Figure S-10 Zr/Y vs La/Y for Reykjanes Ridge (this study) and Stapafell (Peate *et al.*, 2009) basalts. Aggregate fractional melting models (solid and dashed curves) are used to assess plausible mantle lithologies, compositions and melting degrees that could produce the observed melt trace element systematics. Small gold triangles show basalt compositions from Iceland's axial rift zones, compiled from the Icelandic Volcanic rocks Isotopic Database (IVID) of Harðardóttir *et al.* (2022), volcanic zones 1-4, and filtered for basalt composition, 45-52 wt.% SiO_2. These data demonstrate that the Reykjanes Ridge and Stapafell basalts are reasonable endmembers for the compositional array of the Reykjanes Ridge-Iceland plume region.

Incorporating halogens into the partial melting model: Derivation of partition coefficients

We used the results of mineral-melt partitioning experiments from Joachim *et al.* (2015) to define the temperature dependence of chlorine partitioning between olivine and melt, and orthopyroxene and melt:

$$logD_{Cl}^{ol-melt} = 0.00621T(C) - 10.791$$

$$logD_{Cl}^{opx-melt} = 0.00685T(C) - 11.762$$

At any given temperature, $D_{Cl}^{cpx-melt}/D_{Cl}^{opx-melt}$ is about 5, and $D_{Cl}^{gt-melt} \approx D_{Cl}^{opx-melt}$ (Dalou *et al.*, 2012). We are not aware of any experimental studies of chlorine partitioning between spinel and melt, so we have assumed that $D_{Cl}^{sp-melt} \approx D_{Cl}^{opx-melt}$. We are not aware of any published experimental studies of Br and I partitioning between mantle minerals and silicate melt, so for simplicity we have assumed that $D_{Cl}^{bulk} = D_{Br}^{bulk} = D_{I}^{bulk}$.

The mantle potential temperature T_p at the southwest end of the Reykjanes Ridge segment is 1405 °C (Novella *et al.*, 2020), which translates to a lherzolite solidus of ~1480 °C. The mantle potential temperature for our most northeasterly

Reykjanes Ridge sample, closest to Iceland, is 1465 °C (Novella *et al.*, 2020), and at this T_p the garnet pyroxenite solidus is ~1570 °C. We assume that lherzolite-derived melt segregates from its mantle at 1300 °C, and pyroxenite-derived melt segregates from its mantle at 1500 °C (Joachim *et al.*, 2015; Stolper *et al.*, 1981), and use these temperatures to derive bulk partition coefficients for each of the modelled mantle lithologies (Table S-4).

Table S-4 Calculated bulk Cl partition coefficients used in the melting model for Figure 4 of the main text. T_{seg} is the temperature at which melt segregates from its source mantle; *f* is the fraction of each mineral phase in the source lithology; sp = spinel, gt = garnet, ol = olivine, opx = orthopyroxene, cpx = clinopyroxene.

Lithology	T_{seg}, °C	$f_{sp}D_{sp}$	$f_{gt}D_{gt}$	$f_{ol}D_{ol}$	$f_{opx}D_{opx}$	$f_{cpx}D_{cpx}$	$D_{Cl}^{bulk} = \Sigma f_i D_i$
Spinel lherzolite	1300	0.00003	-	0.001	0.0003	0.00005	0.0015
Spinel pyroxenite	1500	0.002	-	0.006	0.005	0.004	0.0171
Garnet lherzolite	1500	-	0.007	0.018	0.006	0.001	0.0307
Garnet pyroxenite	1500	-	0.009	0.008	-	0.003	0.0197

Halogen contents of plausible depleted and enriched mantle endmembers

Endmember enriched and depleted melt halogen contents are identified by regressing the halogen contents of the Reykjanes Ridge samples against the mass fraction of the enriched melt endmember contributing to that sample, using the method of Shorttle *et al*. (2014) as described in the main text (Fig. 4a, Fig. S-11a, Fig. S-12a). We use these endmember melt compositions to constrain the halogen contents of plausible mantle source endmembers. We used the aggregate fractional melting equation to calculate estimates of the Cl, Br and I contents for plausible depleted and enriched mantle endmembers supplying melts to the Reykjanes Ridge. The melting degrees used in the calculations are those that provide reasonable matches to the trace element systematics of Reykjanes Ridge and Stapafell basalts (Fig. S-10), and also match along-ridge variations in crustal thickness (Shorttle *et al.*, 2014). Upper and lower bounds on these melting degrees (Table S-5) are used to estimate plausible upper and lower bounds on the halogen contents for each mantle lithology. The calculated halogen contents of the enriched and depleted mantle endmembers, and the upper and lower bounds on these estimates, are given in Table S-6 and shown on Figures 4b, S-11b, and S-12b. These calculations cannot uniquely identify the mantle source compositions, but they illustrate the key parameters that must be considered to arrive at plausible estimates.

To test the sensitivity of calculated source halogen content to the partition coefficient, we explored the effect of (a) decreasing the melt segregation temperature by 50 °C, and (b) increasing the melt segregation temperature to the liquidus temperature (i.e., instantaneous melt segregation). In all cases, decreasing the melt segregation temperature lowers the calculated partition coefficient, but has no effect on the calculated Cl, Br or I contents of the source lithology. For depleted spinel lherzolite, increasing the melt segregation temperature from 1300 to 1480 °C raises D_{Cl}^{bulk} to 0.021 but has no effect on the calculated Cl, Br or I contents of the source. For the enriched endmember, increasing the melt segregation temperature from 1500 to 1570 °C raises D_{Cl}^{bulk} to 0.050 for spinel pyroxenite, and to 0.057 for garnet pyroxenite. The calculated source Cl contents show a corresponding 6% increase at F=0.15, and 2% increase at F=0.21, but there is no effect on the calculated source Br and I contents.

Table S-5 Bulk partition coefficients D and melt fraction F combinations used to calculate the upper and lower bounds, and preferred estimate, for endmember mantle source halogen contents.

Source	Bound	Lithology	T_{seg}, °C	D_{Cl}^{bulk}	F
Depleted	Lower	Spinel lherzolite	1300	0.0015	0.08
	Preferred	Spinel lherzolite		0.0015	0.1
	Upper	Spinel lherzolite		0.0015	0.12
Enriched	Lower	Spinel pyroxenite	1500	0.017	0.13
	Preferred	Spinel pyroxenite		0.020	0.15
	Upper	Garnet pyroxenite		0.020	0.18

Table S-6 Preferred halogen contents and ratios calculated for depleted and enriched mantle source endmembers, calculated using the preferred melt fractions and partition coefficients given in Table S-5. Lower and upper bounds are given in parentheses. The wide ranges in predicted Br/Cl and I/Cl for the depleted mantle endmember are ultimately controlled by the low but variable Cl contents (57±20 µg/g) measured in the depleted Reykjanes Ridge samples.

Source	Cl, µg/g	Br, ng/g	I, ng/g	Br/Cl $\times 10^{-3}$	I/Cl $\times 10^{-6}$
Depleted	4.2 (1-10)	9.8 (4-17)	0.11 (0.06-0.16)	2.3 (0.7-19)	25.1 (9.6-228)
Enriched	45 (33-61)	106 (77-149)	1.2 (0.8-1.6)	2.4 (1.7-3.3)	26.2 (19-42)

Table S-7 Published halogen contents of key mantle reservoirs and altered oceanic crust, used to generate the compositional ranges shown in Figures 4c, S-11c, and S-12c.

Reference	Cl, µg/g	Br, ng/g	I, ng/g
Proto-Iceland Plume mantle			
N-PIP (depleted): Tomlinson *et al*. (2025)	9.2	104	-
E-PIP (enriched): Tomlinson *et al*. (2025)	20	133	-
Depleted upper mantle			
Recommended: Kendrick (2024)	3 ± 1	8 ± 4	0.2 ± 0.1
Typical range: Kendrick (2024)	1-15	-	-
Primitive mantle			
Kendrick *et al.* (2017)	26 ± 8	76 ± 25	7 ± 4
Altered oceanic crust			
Ito *et al*. (1983)	50 ± 25	-	-
Straub and Layne (2003)	~78	-	-
Chavrit *et al*. (2016)	253^{+436}_{-160}	435^{+729}_{-272}	3^{+11}_{-2}
Barnes *et al*. (2018)	207	150	9
Layer 2: Kendrick (2018)	160^{+140}_{-50}	300^{+300}_{-200}	20^{+20}_{-10}
Layer 3: Kendrick (2018)	360^{+120}_{-60}	700 ± 400	10 ± 10

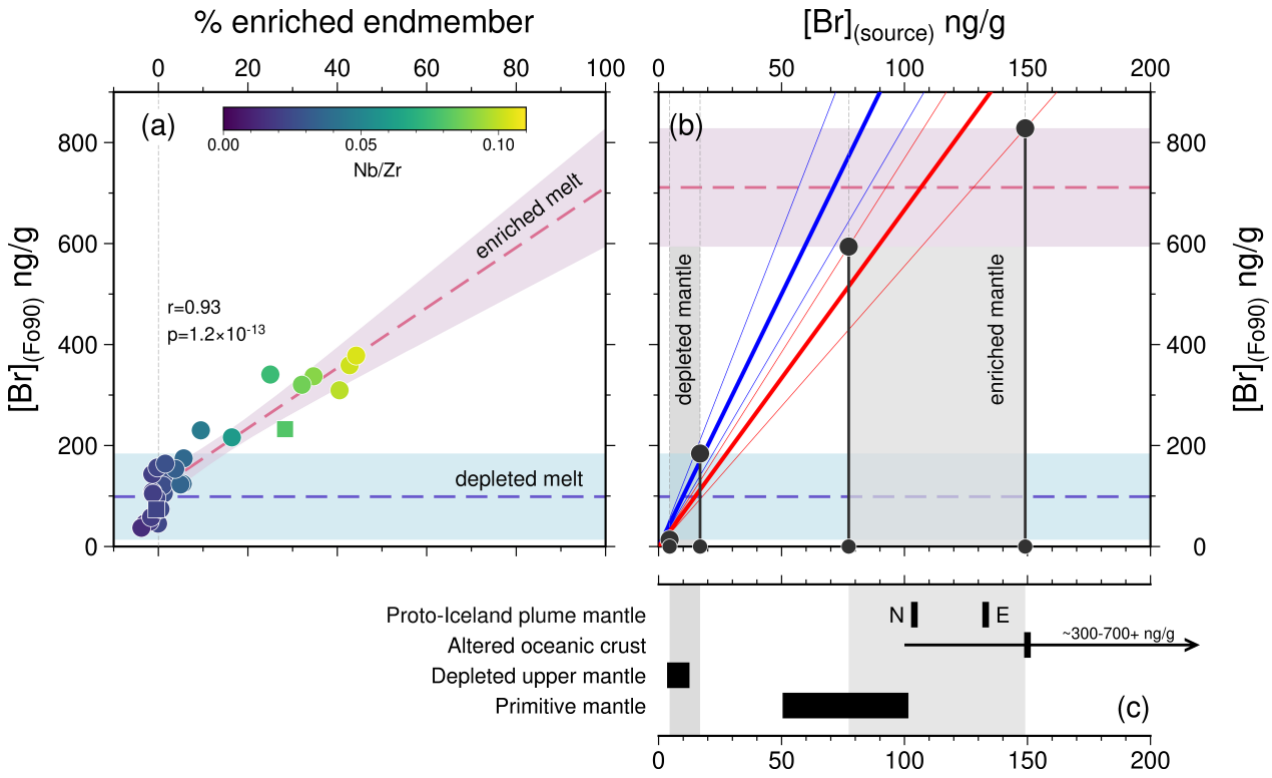


Figure S-11 As Figure 4 in the main text, but for Br.

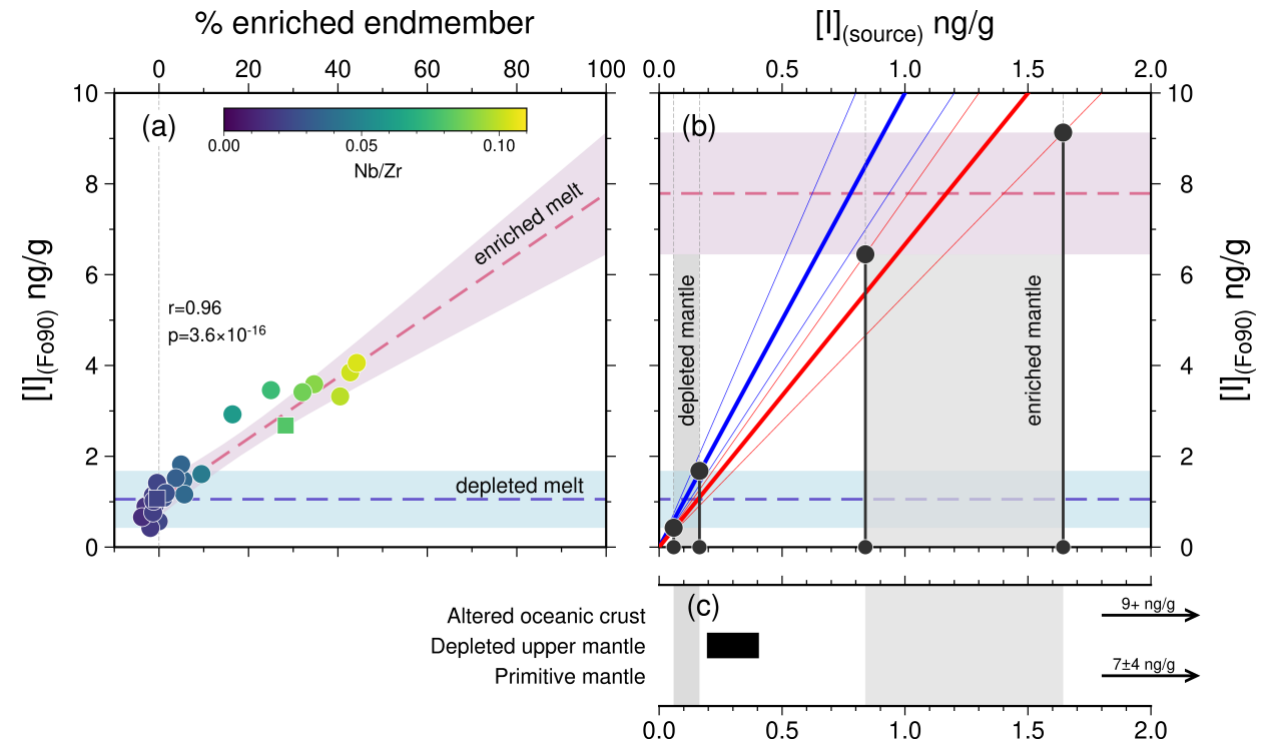


Figure S-12 As Figure 4 in the main text and Figure S-11, but for I.

7. Literature Data Compilations: Reykjanes Ridge, Atlantic and Global MORB

The Cl and Br contents of a different suite of Reykjanes Ridge basalt samples were reported by Unni and Schilling (1978). Their samples were recovered by ocean dredging from locations between 57.6°N and 63.6°N during the TR041 cruise (1976) and the TR100 and TR101 cruises (1971) by the R/V Trident of the University of Rhode Island. Unni and Schilling (1978) show plots of the along-ridge variability in halogen contents, halogen/K and halogen/La ratios, but does not include the geochemical data used to create these plots. Compositional data for the Unni and Schilling (1978) sample set were therefore compiled from the geochemical data reported by Unni (1976) and Schilling *et al.* (1980, 1983) as recorded in PetDB (www.earthchem.org/petdb, accessed 25 April 2024), taking care to select intrinsic halogen values instead of the sum of the intrinsic value plus leachate. The chlorine measurements made on some of these samples have been further discussed by Michael and Cornell (1998). Unfortunately we were unable to discover a complete set of major element data for these samples, so we were unable to calculate a fractionation correction to 10 wt.% MgO.

Reykjanes Ridge basalt compositions were downloaded from PetDB on 7 May 2025 using the Feature Name = Spreading Center = REYKJANES RIDGE, and selecting Classification = Igneous. Data outputs were configured to include one row per sample with any of the following analytes defined: major element oxides, volatiles (H_2O, CO_2, S) isotope ratios ($^{87}Sr/^{86}Sr$, $^{143}Nd/^{144}Nd$, $^{206}Pb/^{204}Pb$, $^{207}Pb/^{204}Pb$, $^{208}Pb/^{204}Pb$, R/R_A), trace elements (Ba, Cr, Nb, Rb, Sr, Y, Zr), rare earth elements La to Lu, and halogens (F, Cl, Br, I). The dataset was filtered by TECTONIC SETTING = SPREADING_CENTER to remove OFF-AXIS samples. We also removed the subset of Cl data attributed to Murton *et al*. (2002); these data are recorded in PetDB as XRF analyses, but are not reported in the original paper nor its supplementary files. Finally, we incorporated additional helium isotope data from Balci *et al*. (2026).

Atlantic and global MORB compositions were downloaded from PetDB on 11 January 2024. The Atlantic MORB dataset was created using the search criterion Feature Name = Spreading Center = MID-ATLANTIC RIDGE, and selecting Classification = Igneous. The global MORB dataset was created using the search criterion Tectonic Setting = SPREADING_CENTER, and selecting Classification = Igneous. Data outputs were configured to include one row per sample with any of the following analytes defined: major element oxides, H_2O wt.%, La ppm, and halogens (F, Cl, Br, I). Both datasets were then filtered by Rock Name = BASALT or THOLEIITE, and samples with no reported Cl, Br or I contents were removed. Remaining data were checked to ensure that Cl, Br and I were reported in consistent units, converting to µg/g (Cl) or ng/g (Br, I) when necessary. The resulting compilations include a small number of samples with very high reported Cl, Br and/or I contents that could indicate assimilation of saline brines, low-temperature seawater alteration, or microbial alteration. We did not perform any filtering to exclude these potentially altered samples. Likewise, we did not filter out samples with extremely low reported halogen contents that could be affected by degassing. We consider that the calculated mean Cl, Br and I contents for the Atlantic and global MORB compilations are likely skewed towards high values, and that the median Cl, Br and I values offer a better representation of the data: in all cases the median lies closer to the peak in the probability distribution (Fig. 1 of the main text) than the mean.

Supplementary Tables

Table S-8 Tab 1 "All_data": Neutron irradiation noble gas mass spectrometry (NI-NGMS) datasheet showing raw measurements of noble gas isotopes and parent halogen contents calculated using the expressions given in Table S-1. Tab 2 "Final_data": Measured NI-NGMS-derived K, Ca, Cl, Br and I contents and 1σ uncertainties for each Reykjanes Ridge sample. Tab 3 "Expressions": irradiation parameters.

Table S-9 Halogen (Cl, Br, I) and K contents, and 1σ analytical uncertainties, for Reykjanes Ridge basalt glasses. Includes: measured halogen abundances; halogens corrected for degassing or alteration; halogen and K abundances corrected to 10 wt.% MgO; halogen and K abundances corrected to a melt composition in equilibrium with Fo_{90} olivine. Relevant major and trace element data used in the study, including to create figures, are also reported in the data sheet: Bulk-rock major and trace elements from Murton *et al*. (2002); lithophile isotope data from Hilton *et al.* (2000), Murton *et al.* (2002) and Thirlwall *et al.* (2004); glass trace elements from Novella *et al.* (2020); glass major elements and proportion of pyroxenite-derived melt from Shorttle *et al.* (2015); glass H_2O contents from Nichols *et al.* (2002).

Tables S-8 and S-9 (xlsx) are available for download from the online version of this article at https://doi.org/10.7185/geochemlet.2640.

Supplementary Information References

Aigner-Torres, M., Blundy, J., Ulmer, P., Pettke, T. (2007) Laser Ablation ICPMS study of trace element partitioning between plagioclase and basaltic melts: an experimental approach. *Contributions to Mineralogy and Petrology* 153, 647–667. https://doi.org/10.1007/s00410-006-0168-2

Balci, U., Di Nicola, L., Fitton, J.G., Taylor, R.N., Stuart, F.M. (2026) Tracking deep mantle heat and volatiles in the Iceland plume from a high-density survey of helium isotopes along the Reykjanes Ridge. *Earth and Planetary Science Letters* 679, 119882. https://doi.org/10.1016/j.epsl.2026.119882

Barnes, J.D., Manning, C.E., Scambelluri, M., Selverstone, J. (2018) The Behavior of Halogens During Subduction-Zone Processes. In: Harlov, D.E., Aranovich, L. (Eds.) *The Role of Halogens in Terrestrial and Extraterrestrial Geochemical Processes: Surface, Crust, and Mantle*. Springer Geochemistry, Cham, 545–590. https://doi.org/10.1007/978-3-319-61667-4_8

Berry, A.J., O'Neill, H.St.C. (2021) Oxygen Content, Oxygen Fugacity, the Oxidation State of Iron, and Mid-Ocean Ridge Basalts. In: Moretti, R., Neuville, D.R. (Eds.) *Magma Redox Geochemistry*. American Geophysical Union and Wiley, Hoboken, 155–163. https://doi.org/10.1002/9781119473206.ch8

Brazzle, R.H., Pravdivtseva, O.V., Meshik, A.P., Hohenberg, C.M. (1999) Verification and interpretation of the I-Xe chronometer. *Geochimica et Cosmochimica Acta* 63, 739–760. https://doi.org/10.1016/S0016-7037(98)00314-7

Brown, E.L., Lesher, C.E. (2016) REEBOX PRO: A forward model simulating melting of thermally and lithologically variable upwelling mantle. *Geochemistry, Geophysics, Geosystems* 17, 3929–3968. https://doi.org/10.1002/2016GC006579

Chavrit, D., Burgess, R., Sumino, H., Teagle, D.A.H., Droop, G., Shimizu, A., Ballentine, C.J. (2016) The contribution of hydrothermally altered ocean crust to the mantle halogen and noble gas cycles. *Geochimica et Cosmochimica Acta* 183, 106–124. https://doi.org/10.1016/j.gca.2016.03.014

Dalou, C., Koga, K.T., Shimizu, N., Boulon, J., Devidal, J.-L. (2012) Experimental determination of F and Cl partitioning between lherzolite and basaltic melt. *Contributions to Mineralogy and Petrology* 163, 591–609. https://doi.org/10.1007/s00410-011-0688-2

Danyushevsky, L.V. (2001) The effect of small amounts of H_2O on crystallisation of mid-ocean ridge and backarc basin magmas. *Journal of Volcanology and Geothermal Research* 110, 265–280. https://doi.org/10.1016/S0377-0273(01)00213-X

Danyushevsky, L.V., Plechov, P. (2011) Petrolog3: Integrated software for modeling crystallization processes. *Geochemistry, Geophysics, Geosystems* 12, Q07021. https://doi.org/10.1029/2011GC003516

German, C.R., Briem, J., Chin, C., Danielsen, M., Holland, S., *et al.* (1994) Hydrothermal activity on the Reykjanes Ridge: the Steinahóll vent-field at 63°06′N. *Earth and Planetary Science Letters* 121, 647–654. https://doi.org/10.1016/0012-821X(94)90098-1

Gilmour, J.D., Pravdivtseva, O.V., Busfield, A., Hohenberg, C.M. (2006) The I-Xe chronometer and the early solar system. *Meteoritics & Planetary Science* 41, 19–31. https://doi.org/10.1111/j.1945-5100.2006.tb00190.x

Harðardóttir, S., Matthews, S., Halldórsson, S.A., Jackson, M.G. (2022) Spatial distribution and geochemical characterization of Icelandic mantle end-members: Implications for plume geometry and melting processes. *Chemical Geology* 604, 120930. https://doi.org/10.1016/j.chemgeo.2022.120930

Hart, S.R., Dunn, T. (1993) Experimental cpx/melt partitioning of 24 trace elements. *Contributions to Mineralogy and Petrology* 113, 1–8. https://doi.org/10.1007/BF00320827

Hartley, M.E., de Hoog, J.C.M., Shorttle, O. (2021) Boron isotopic signatures of melt inclusions from North Iceland reveal recycled material in the Icelandic mantle source. *Geochimica et Cosmochimica Acta* 294, 273–294. https://doi.org/10.1016/j.gca.2020.11.013

Herzberg, C., O'Hara, M.J. (2002) Plume-Associated Ultramafic Magmas of Phanerozoic Age. *Journal of Petrology* 43, 1857–1883. https://doi.org/10.1093/petrology/43.10.1857

Hilton, D.R., Thirlwall, M.F., Taylor, R.N., Murton, B.J., Nichols, A. (2000) Controls on magmatic degassing along the Reykjanes Ridge with implications for the helium paradox. *Earth and Planetary Science Letters* 183, 43–50. https://doi.org/10.1016/S0012-821X(00)00253-3

Ito, E., Harris, D.M., Anderson, Jr., A.T. (1983) Alteration of oceanic crust and geologic cycling of chlorine and water. *Geochimica et Cosmochimica Acta* 47, 1613–1624. https://doi.org/10.1016/0016-7037(83)90188-6

Joachim, B., Pawley, A., Lyon, I.C., Marquardt (neé Hartmann), K., Henkel, T., Clay, P.L., Ruzié, L., Burgess, R., Ballentine, C.J. (2015) Experimental partitioning of F and Cl between olivine, orthopyroxene and silicate melt at Earth's mantle conditions. *Chemical Geology* 416, 65–78. https://doi.org/10.1016/j.chemgeo.2015.08.012

Joachim, B., Stechern, A., Ludwig, T., Konzett, J., Pawley, A., Ruzié-Hamilton, L., Clay, P.L., Burgess, R., Ballentine, C.J. (2017) Effect of water on the fluorine and chlorine partitioning behavior between olivine and silicate melt. *Contributions to Mineralogy and Petrology* 172, 15. https://doi.org/10.1007/s00410-017-1329-1

Jones, S.M., Murton, B.J., Fitton, J.G., White, N.J., Maclennan, J., Walters, R.L. (2014) A joint geochemical–geophysical record of time-dependent mantle convection south of Iceland. *Earth and Planetary Science Letters* 386, 86–97. https://doi.org/10.1016/j.epsl.2013.09.029

Kendrick, M.A. (2012) High precision Cl, Br and I determinations in mineral standards using the noble gas method. *Chemical Geology* 292–293, 116–126. https://doi.org/10.1016/j.chemgeo.2011.11.021

Kendrick, M.A. (2018) Halogens in Seawater, Marine Sediments and the Altered Oceanic Lithosphere. In: Harlov, D.E., Aranovich, L. (Eds.) *The Role of Halogens in Terrestrial and Extraterrestrial Geochemical Processes: Surface, Crust, and Mantle*. Springer Geochemistry, Cham, 591–648. https://doi.org/10.1007/978-3-319-61667-4_9

Kendrick, M.A. (2019) Halogens in altered ocean crust from the East Pacific Rise (ODP/IODP Hole 1256D). *Geochimica et Cosmochimica Acta* 261, 93–112. https://doi.org/10.1016/j.gca.2019.06.044

Kendrick, M.A. (2024) Halogen Cycling in the Solid Earth. *Annual Review of Earth and Planetary Sciences* 52, 195–220. https://doi.org/10.1146/annurev-earth-031621-111700

Kendrick, M.A., Arculus, R., Burnard, P., Honda, M. (2013) Quantifying brine assimilation by submarine magmas: Examples from the Galápagos Spreading Centre and Lau Basin. *Geochimica et Cosmochimica Acta* 123, 150–165. https://doi.org/10.1016/j.gca.2013.09.012

Kendrick, M.A., Honda, M., Vanko, D.A. (2015a) Halogens and noble gases in Mathematician Ridge meta-gabbros, NE Pacific: implications for oceanic hydrothermal root zones and global volatile cycles. *Contributions to Mineralogy and Petrology* 170, 43. https://doi.org/10.1007/s00410-015-1192-x

Kendrick, M.A., Jackson, M.G., Hauri, E.H., Phillips, D. (2015b) The halogen (F, Cl, Br, I) and H_2O systematics of Samoan lavas: Assimilated-seawater, EM2 and high-$^3He/^4He$ components. *Earth and Planetary Science Letters* 410, 197–209. https://doi.org/10.1016/j.epsl.2014.11.026

Kendrick, M.A., Hémond, C., Kamenetsky, V.S., Danyushevsky, L., Devey, C.W., Rodemann, T., Jackson, M.G., Perfit, M.R. (2017) Seawater cycled throughout Earth's mantle in partially serpentinized lithosphere. *Nature Geoscience* 10, 222–228. https://doi.org/10.1038/ngeo2902

Kendrick, M.A., Nebel, O., Hanyu, T., Maunder, B.L., Maas, R. (2025) Earth's early differentiation recorded by halogen abundance ratios in Hawaiian lavas. *Geochimica et Cosmochimica Acta* 393, 196–207. https://doi.org/10.1016/j.gca.2025.01.019

Li, Y.-H. (1991) Distribution patterns of the elements in the ocean: A synthesis. *Geochimica et Cosmochimica Acta* 55, 3223–3240. https://doi.org/10.1016/0016-7037(91)90485-N

Michael, P.J., Cornell, W.C. (1998) Influence of spreading rate and magma supply on crystallization and assimilation beneath mid-ocean ridges: Evidence from chlorine and major element chemistry of mid-ocean ridge basalts. *Journal of Geophysical Research: Solid Earth* 103, 18325–18356. https://doi.org/10.1029/98JB00791

Murton, B.J. (1995) *RSS Charles Darwin Cruise CD80, 01 Sep - 01 Oct 1993. The PETROS Programme*. Institute of Oceanographic Sciences, Deacon Laboratory Cruise Report 241, Wormley, UK.

Murton, B.J., Taylor, R.N., Thirlwall, M.F. (2002) Plume–Ridge Interaction: a Geochemical Perspective from the Reykjanes Ridge. *Journal of Petrology* 43, 1987–2012. https://doi.org/10.1093/petrology/43.11.1987

Nichols, A.R.L., Carroll, M.R., Höskuldsson, Á. (2002) Is the Iceland hot spot also wet? Evidence from the water contents of undegassed submarine and subglacial pillow basalts. *Earth and Planetary Science Letters* 202, 77–87. https://doi.org/10.1016/S0012-821X(02)00758-6

Novella, D., Maclennan, J., Shorttle, O., Prytulak, J., Murton, B.J. (2020) A multi-proxy investigation of mantle oxygen fugacity along the Reykjanes Ridge. *Earth and Planetary Science Letters* 531, 115973. https://doi.org/10.1016/j.epsl.2019.115973

Palme, H., O'Neill, H.St.C. (2014) Cosmochemical Estimates of Mantle Composition. In: Holland, H.D., Turekian, K.K. (Eds.) *Treatise on Geochemistry. Volume 3: The Mantle and Core*. Elsevier, Amsterdam, 1–39. https://doi.org/10.1016/B978-0-08-095975-7.00201-1

Peate, D.W., Baker, J.A., Jakobsson, S.P., Waight, T.E., Kent, A.J.R., Grassineau, N.V., Skovgaard, A.C. (2009) Historic magmatism on the Reykjanes Peninsula, Iceland: a snap-shot of melt generation at a ridge segment. *Contributions to Mineralogy and Petrology* 157, 359–382. https://doi.org/10.1007/s00410-008-0339-4

Philpotts, J.A., Schnetzler, C.C. (1970) Phenocryst-matrix partition coefficients for K, Rb, Sr and Ba, with applications to anorthosite and basalt genesis. *Geochimica et Cosmochimica Acta* 34, 307–322. https://doi.org/10.1016/0016-7037(70)90108-0

Renne, P.R., Balco, G., Ludwig, K.R., Mundil, R., Min, K. (2011) Response to the comment by W.H. Schwarz *et al.* on "Joint determination of ^{40}K decay constants and ^{40}Ar*/^{40}K for the Fish Canyon sanidine standard, and improved accuracy for ^{40}Ar/^{39}Ar geochronology" by P.R. Renne *et al.* (2010). *Geochimica et Cosmochimica Acta* 75, 5097–5100. https://doi.org/10.1016/j.gca.2011.06.021

Roddick, J.C. (1983) High precision intercalibration of ^{40}Ar-^{39}Ar standards. *Geochimica et Cosmochimica Acta* 47, 887–898. https://doi.org/10.1016/0016-7037(83)90154-0

Ruzié-Hamilton, L., Clay, P.L., Burgess, R., Joachim, B., Ballentine, C.J., Turner, G. (2016) Determination of halogen abundances in terrestrial and extraterrestrial samples by the analysis of noble gases produced by neutron irradiation. *Chemical Geology* 437, 77–87. https://doi.org/10.1016/j.chemgeo.2016.05.003

Salters, V.J.M., Stracke, A. (2004) Composition of the depleted mantle. *Geochemistry, Geophysics, Geosystems* 5, Q05B07. https://doi.org/10.1029/2003GC000597

Schilling, J.-G., Bergeron, M.B., Evans, R. (1980) Halogens in the mantle beneath the North Atlantic. *Philosophical Transactions of the Royal Society of London. Series A, Mathematical and Physical Sciences* 297, 147–178. https://doi.org/10.1098/rsta.1980.0208

Schilling, J.-G., Zajac, M., Evans, R., Johnston, T., White, W., Devine, J.D., Kingsley, R. (1983) Petrologic and geochemical variations along the Mid-Atlantic Ridge from 29 degrees N to 73 degrees N. *American Journal of Science* 283, 510–586. https://doi.org/10.2475/ajs.283.6.510

Shorttle, O., Maclennan, J. (2011) Compositional trends of Icelandic basalts: Implications for short–length scale lithological heterogeneity in mantle plumes. *Geochemistry, Geophysics, Geosystems* 12, Q11008. https://doi.org/10.1029/2011GC003748

Shorttle, O., Maclennan, J., Lambart, S. (2014) Quantifying lithological variability in the mantle. *Earth and Planetary Science Letters* 395, 24–40. https://doi.org/10.1016/j.epsl.2014.03.040

Shorttle, O., Moussallam, Y., Hartley, M.E., Maclennan, J., Edmonds, M., Murton, B.J. (2015) Fe-XANES analyses of Reykjanes Ridge basalts: Implications for oceanic crust's role in the solid Earth oxygen cycle. *Earth and Planetary Science Letters* 427, 272–285. https://doi.org/10.1016/j.epsl.2015.07.017

Steiger, R.H., Jäger, E. (1977) Subcommission on geochronology: Convention on the use of decay constants in geo- and cosmochronology. *Earth and Planetary Science Letters* 36, 359–362. https://doi.org/10.1016/0012-821X(77)90060-7

Stolper, E., Walker, D., Hager, B.H., Hays, J.F. (1981) Melt segregation from partially molten source regions: The importance of melt density and source region size. *Journal of Geophysical Research: Solid Earth* 86, 6261–6271. https://doi.org/10.1029/JB086iB07p06261

Stracke, A., Bizimis, M., Salters, V.J.M. (2003) Recycling oceanic crust: Quantitative constraints. *Geochemistry, Geophysics, Geosystems* 4, 8003. https://doi.org/10.1029/2001GC000223

Straub, S.M., Layne, G.D. (2003) The systematics of chlorine, fluorine, and water in Izu arc front volcanic rocks: Implications for volatile recycling in subduction zones. *Geochimica et Cosmochimica Acta* 67, 4179–4203. https://doi.org/10.1016/S0016-7037(03)00307-7

Templeton, A.S., Staudigel, H., Tebo, B.M. (2005) Diverse Mn(II)-Oxidizing Bacteria Isolated from Submarine Basalts at Loihi Seamount. *Geomicrobiology Journal* 22, 127–139. https://doi.org/10.1080/01490450590945951

Thirlwall, M.F., Gee, M.A.M., Taylor, R.N., Murton, B.J. (2004) Mantle components in Iceland and adjacent ridges investigated using double-spike Pb isotope ratios. *Geochimica et Cosmochimica Acta* 68, 361–386. https://doi.org/10.1016/S0016-7037(03)00424-1

Tomlinson, E.L., Rose-Koga, E.F., Bouvier, A.-S., O'Farrell, D., Caulfield, J.T., Jackson, M.G., Moussallam, Y., Stuart, F.M., Villeneuve, J. (2025) Halogens in proto-Iceland plume basalts. *Geochemical Perspectives Letters* 37, 12–17. https://doi.org/10.7185/geochemlet.2539

Toplis, M.J. (2005) The thermodynamics of iron and magnesium partitioning between olivine and liquid: criteria for assessing and predicting equilibrium in natural and experimental systems. *Contributions to Mineralogy and Petrology* 149, 22–39. https://doi.org/10.1007/s00410-004-0629-4

Turner, G., Huneke, J.C., Podosek, F.A., Wasserburg, G.J. (1971) ^{40}Ar-^{39}Ar ages and cosmic ray exposure ages of Apollo 14 samples. *Earth and Planetary Science Letters* 12, 19–35. https://doi.org/10.1016/0012-821X(71)90051-3

Unni, C.K. (1976) *Chlorine and bromine degassing during submarine and subaerial volcanism*. PhD thesis, University of Rhode Island.

Unni, C.K., Schilling, J.-G. (1978) Cl and Br degassing by volcanism along the Reykjanes Ridge and Iceland. *Nature* 272, 19–23. https://doi.org/10.1038/272019a0

Wijbrans, J.R. (1985) *Geochronology of metamorphic terrains by the $^{40}Ar/^{39}Ar$ age spectrum method*. PhD thesis, Australian National University.

Workman, R.K., Hart, S.R. (2005) Major and trace element composition of the depleted MORB mantle (DMM). *Earth and Planetary Science Letters* 231, 53–72. https://doi.org/10.1016/j.epsl.2004.12.005